

Can't Touch This: Real-Time, Safe Motion Planning and Control for Manipulators Under Uncertainty

Jonathan Michaux¹, Patrick Holmes¹, Bohao Zhang¹, Che Chen¹, Baiyue Wang¹, Shrey Sahgal¹, Tiancheng Zhang¹, Sidhartha Dey⁴, Shreyas Kousik², and Ram Vasudevan^{1,3}

Abstract—A key challenge to the widespread deployment of robotic manipulators is the need to ensure safety in arbitrary environments while generating new motion plans in real-time. In particular, one must ensure that a manipulator does not collide with obstacles, collide with itself, or exceed its joint torque limits. This challenge is compounded by the need to account for uncertainty in the mass and inertia of manipulated objects, and potentially the robot itself. The present work addresses this challenge by proposing Autonomous Robust Manipulation via Optimization with Uncertainty-aware Reachability (ARMOUR), a provably-safe, receding-horizon trajectory planner and tracking controller framework for serial link manipulators. ARMOUR works by first constructing a robust, passivity-based controller that is proven to enable a manipulator to track desired trajectories with bounded error despite uncertain dynamics. Next, ARMOUR uses a novel variation on the Recursive Newton-Euler Algorithm (RNEA) to compute the set of all possible inputs required to track any trajectory within a continuum of desired trajectories. Finally, the method computes an over-approximation to the swept volume of the manipulator; this enables one to formulate an optimization problem, which can be solved in real-time, to synthesize provably-safe motion. The proposed method is compared to state of the art methods and demonstrated on a variety of challenging manipulation examples in simulation and on real hardware, such as maneuvering a dumbbell with uncertain mass around obstacles.

I. INTRODUCTION

Robotic manipulators have the potential to assist humans in a wide variety of collaborative settings, such as manufacturing, package delivery, and in-home care. However, such settings are typically constrained and uncertain; nevertheless, the robot must operate in a safety-critical fashion. This makes it challenging to directly apply high-torque manipulators that can ignore uncertainty due to their own mass and the mass of manipulated objects. Instead, it is necessary to develop motion planning and control strategies that can operate safely by accounting for these types of uncertainty in real-time. In this context, safety means avoiding collisions while obeying joint position, velocity, and torque limits.

This work is supported by the Ford Motor Company via the Ford-UM Alliance under award N022977, National Science Foundation Career Award #1751093 and by the Office of Naval Research under Award Number N00014-18-1-2575

¹Robotics Institute, University of Michigan, Ann Arbor, MI (jmmichaux, pdholmes, jimzhang, ramv, cctom, baiyuew, shreyas, zhangtc)@umich.edu.

²Mechanical Engineering, Georgia Institute of Technology, Atlanta, GA shreyas.kousik@me.gatech.edu.

³Mechanical Engineering, University of Michigan, Ann Arbor, MI (ramv)@umich.edu.

⁴Agility Robotics, Albany, OR (sid.dey)@agilityrobotics.com.

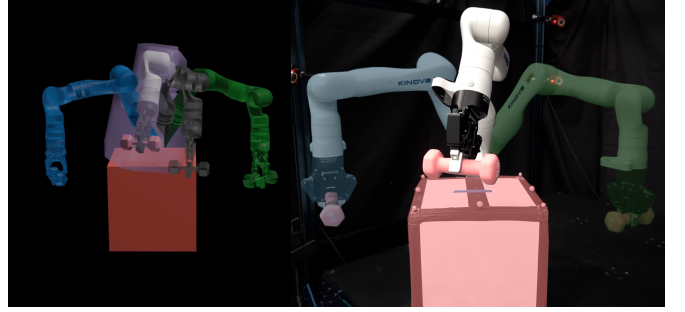


Fig. 1. An overview of the proposed method entitled ARMOUR. This paper considers the problem of safe motion planning with uncertain dynamics; for example, when manipulating a heavy dumbbell (pink) with uncertain mass in clutter (red obstacles). ARMOUR operates in a receding horizon way, moving from the start (right panel, blue) arm to the goal (right panel, green arm) by repeatedly generating new trajectory plans in real time. In each planning iteration, ARMOUR first computes a Forward Reachable Set (FRS) for a continuum of possible motion plans (left panel, purple volume), representing the swept volume of the arm under uncertain dynamics. Many of these motion plans may be in collision, so ARMOUR solves a constrained trajectory optimization problem to find a collision-free plan that makes progress towards an intermediate waypoint (left panel, black arm) and the global goal (right panel, green arm).

To address the safety challenge, this paper proposes **Autonomous Robust Manipulation via Optimization with Uncertainty-aware Reachability (ARMOUR)**, a method for guaranteed-safe, real-time manipulator motion planning and control. An overview of this method is given in Fig. 1. The present work enables safety for uncertain manipulator dynamics, which includes uncertain payloads, by proposing a combined planning and control framework. To proceed, we outline our research scope, state the contributions of this paper, and present a brief overview of the proposed method and the remainder of the paper.

The focus of this paper is manipulator planning and control under uncertainty in a robot's dynamic model. Typically, one relies on an accurate model of the robot that is assumed to be true. However, no model is perfect, and a model's properties may be uncertain. For example, the dynamics of a robotic arm depend on potentially uncertain inertial properties: link masses, center of mass locations, and inertia matrices. Similarly, a manipulator may not have access to an object's true inertial properties when grasping and transporting it. This work seeks to robustly account for set-based uncertainty in manipulator and object inertial properties.

Safety is a critical property for deploying manipulators in real-world scenarios, as collisions with people or objects (i.e., obstacles) could cause grave harm. Planning and control for collision avoidance is challenging because most obstacle-

avoidance constraints are non-convex, and manipulators typically have nonlinear dynamics. This challenge is compounded by the need to obey position, velocity, and torque constraints at each joint to avoid damaging the robot. Furthermore, it is necessary to guarantee safety in continuous time, to ensure no safety violations between discrete time steps. This work ensures safety by making continuous-time guarantees on collision avoidance, actuator limits, joint position limits, and joint velocity limits. Because mobile robots must update their maps of the world as they move and collect new information, this work focuses on the development of a real-time, receding horizon planning and control method.

Contribution: To the best of our knowledge, no motion planning and control framework exists which guarantees the continuous time safety of a manipulator robot with set-based uncertainty and operates in real time. Our framework guarantees continuous time collision avoidance and satisfaction of a robot’s torque bounds and joint limits while explicitly accounting for tracking error caused by uncertainty in the robot’s dynamics. We make the following contributions. First, we propose a novel robust passivity-based controller to safely account for uncertain robot dynamics by providing explicit tracking error guarantees. Second, we provide a novel variation of the modified Recursive Newton-Euler Algorithm (RNEA) [1], which we call polynomial zonotope RNEA (PZRNEA). This approach uses polynomial zonotopes [2] to compute sets of possible inputs required to track trajectories, and allows us to satisfy torque limit constraints during motion planning. Third, we use polynomial zonotopes to represent the forward occupancy of the robot, which is used to guarantee obstacle avoidance. Each of these contributions is used to formulate the motion planning and control problem as an optimization problem that can be tractably solved in real-time with formal safety guarantees in a receding horizon fashion. We demonstrate our method in simulation and hardware and compare it to state of the art alternatives. These experiments confirm that our method enables safe manipulation of grasped objects with uncertain inertial parameters, while other methods may cause collisions or require movements that are physically unachievable.

Improvement Over Our Prior Work: ARMOUR builds upon prior work entitled Autonomous, Reachability-based Manipulator Trajectory Design (ARMTD) [3]. This prior work focused on performing autonomous manipulator planning for deterministic kinematic models. In contrast, the current presented work is able to account for model uncertainty while using a dynamic model of the manipulator. Furthermore, ARMOUR significantly reduces the conservativeness of ARMTD’s numerical reachable set representation by using polynomial zonotopes. Lastly, in contrast to ARMTD, ARMOUR describes a strategy for control design and is able to account for input constraints.

Method and Paper Overview: First, we review related work in Sec. II. Next, relevant notation and mathematical objects are introduced in Sec. III, and the robot’s kinematics, dynamics and environment are discussed in Sec. IV. Our motion planning and control hierarchy operates in a receding-horizon fashion, and is split into three levels: a high-level

planner (HLP), a mid-level safe trajectory planner, and a low-level robust controller. We implement a robust passivity-based controller that uniformly bounds the tracking performance despite uncertainty in the robot’s dynamics (Sec. VII). Our framework plans in terms of parameterized desired trajectories of each joint (Sec. VI). Online, these are assembled into reachable sets of the full arm to bound the robot’s motion through the workspace and utilized within PZRNEA to bound the inputs required to track any desired trajectory (Sec. VIII). Torque constraints and obstacle collision-avoidance constraints guarantee the safety of our method within an online trajectory optimization program (Sec. IX), which generates a desired trajectory to be tracked by the robust controller. The cost function of the optimization program may be designed based on output from a high-level planner, such as reaching a desired waypoint. We then demonstrate the efficacy of our method for safely manipulating uncertain grasped objects in simulation and in the real-world, and we compare it to other state of the art methods (Sec. X) We conclude and describe future work in Sec. XI.

II. BACKGROUND AND RELATED WORK

This paper addresses the problem of real-time, safe manipulation planning and control that accounts for uncertain dynamics. A common approach to solving similar problems is to use a global, sampling-based path planner to generate coarse, high-level motions, then a local planner to generate trajectories, and finally a controller to track the trajectories (e.g., [4], [5], and our own prior work [3], [6]). We now review methods for both planning and control.

A. Planning

It is challenging to generate motion plans to complete tasks while obeying constraints in real time due to the high-dimensional models typically used to describe manipulators. Planning methods can be categorized depending upon how physics are represented: one can ignore physics (i.e., path or kinematic planning), or represent dynamics. Methods can also be categorized by how plans are synthesized, using either sampling (e.g., [7], [8]) or optimization (e.g., [9], [10]). Note, further categorization can be applied depending upon how the robot and its environment are represented [11], [12]. Recall that the present work considers real-time, optimization-based motion planning for manipulators with uncertain dynamics. To proceed, we review how kinematics, dynamics, and uncertainty have been considered in sampling- and optimization-based approaches; note that a thorough survey is available [12].

A common approach to enable fast performance is to plan a path or a kinematic trajectory, then rely on an underlying feedback controller to compensate for the robot’s true dynamics. Our previous work [3] employed this strategy, as do a variety of optimization-based planners [9], [10], [13]. This approach is also used in sampling-based motion planning for complex robots such as manipulators or humanoids, often by directly modeling the configuration manifold [14], [15], though these approaches are not typically fast enough for real time replanning. To increase computational efficiency, one can

instead precompute some constraint manifolds [16]. With these methods, computational speed comes at the expense of not modeling the dynamics of the robot.

An alternate approach is to incorporate a model of the robot's dynamics during planning. Notably, in the manipulator literature, Berenson et al. [17] extend the well-known Rapidly-exploring Random Trees (RRT) algorithm [18] to incorporate torque and friction constraints in discrete time by projection to constraint manifolds, though this approach cannot plan in real time. More recently, it has been shown how to verify robot motion near humans by rapidly computing capsule-shaped safety zones for manipulator dynamics [19]–[21]; however, these methods do not appear to account for uncertainty in the dynamics. These previous methods focus on collision avoidance for manipulators; however, we briefly note that there is extensive work on humanoid motion planning with dynamics, typically by planning a sequence of static, dynamically-feasible poses [22]–[24]. These latter methods do not operate in real time due to the high-dimensional nature of humanoid robots. Altogether, it remains a challenge to rapidly plan collision-free manipulator motion while incorporating uncertain dynamics.

B. Control

As mentioned above, to achieve fast performance, most approaches plan kinematic paths or trajectories, then rely on a lower-level controller to obey dynamic constraints. We briefly note that some approaches instead merge kinematic planning and control [25], [26] by generalizing the notion of potential fields. These concepts can also extend to multi-manipulator systems [27] and humanoids [28]. While these methods can guarantee kinematic collision avoidance in discrete time [26], they do not incorporate dynamics. To proceed, we review classical adaptive methods, and more recent interval arithmetic methods, for robust manipulator control.

There is a long history of control strategies that seek to account for manipulator dynamics [29], including nonlinear actuator models and flexible links [30]. The core challenge is to develop robust controllers that guarantee convergence to a given desired trajectory despite disturbance and uncertain, nonlinear dynamics. A further challenge is to ensure these controllers are continuous, to avoid chattering or exciting high-frequency dynamics that are not typically modeled [31], [32]. To handle parametric uncertainty, a variety of adaptive and sliding-mode control approaches have been proposed that prove both convergence and bounds on trajectory tracking error by simultaneously controlling a robot and estimating its uncertain parameters; such techniques were originally introduced in the 1980s and continue to be developed through the past decade [33]–[36].

One of the key challenges with such techniques is to estimate bounds on the nonlinear perturbations to the controlled system [34]. Thus, a recent alternative has been to directly compute the reachable set of states for a manipulator with parameter uncertainty via interval arithmetic [37]–[39], building off of existing techniques for linear systems (e.g., [40], [41]) and nonlinear systems (e.g., [42], [43]). In the present work,

we develop a novel controller with tighter bounds based on these previous interval arithmetic methods (as is discussed in Appendix F).

III. PRELIMINARIES

This work performs safe motion planning by conservatively representing the swept volume of a manipulator subject to uncertain dynamics. To achieve this, we leverage several numerical set representations of increasing complexity: intervals, zonotopes, and polynomial zonotopes. In this section, we describe our notation conventions, then describe each set representation and its significance in our overall framework.

A. Notation

The n -dimensional real numbers are \mathbb{R}^n , natural numbers \mathbb{N} , the unit circle is \mathbb{S}^1 , and the set of 3×3 orthonormal matrices is $\text{SO}(3)$. Subscripts may index elements of a vector or a set, or provide additional context. For a matrix A , we use A^\top to denote its transpose. We use the product notation $\prod_{i=1}^m A_i = A_1 A_2 \cdots A_m$ to denote successive matrix multiplications, where each $A_i \in \mathbb{R}^{n \times n}$. Vector concatenation is denoted (x_1, \dots, x_n) unless the shape is critical to understanding, in which case we write $[x_1^\top, \dots, x_n^\top]^\top$.

Let $U, V \subset \mathbb{R}^n$. For a point $u \in U$, $\{u\} \subset U$ is the set containing only u . The *power set* of U is $\text{pow}(U)$. The *Minkowski Sum* is $U \oplus V = \{u + v \mid u \in U, v \in V\}$; the *Minkowski difference* is $U \ominus V = U \oplus (-V)$. For vectors $a, b \in \mathbb{R}^3$, we write the cross product $a \times b$ as $a^\times b$, where

$$a^\times = \begin{bmatrix} 0 & -a_3 & a_2 \\ a_3 & 0 & -a_1 \\ -a_2 & a_1 & 0 \end{bmatrix}. \quad (1)$$

If $n = 3$, the *set-based cross product* is defined as $U \otimes V = \{u \times v \mid u \in U, v \in V\}$. If $\{U_i \subset \mathbb{R}^n\}_{i=1}^m$ then let $\times_{i=1}^m U_i$ denote the Cartesian product of the U_i 's. Let $W \subset \mathbb{R}^{n \times n}$ be a set of square matrices. Then, *set-based multiplication* is defined as $WV = \{Av, \mid A \in W, v \in V\}$. Let 0 (resp. I) denote a matrix of zeros (resp. ones) of appropriate size, and let I_n be the $n \times n$ identity matrix.

B. Intervals

We describe uncertain manipulator parameters using intervals (see [44] or [45] for an overview of interval arithmetic). An n -dimensional interval is a set

$$[x] = \{y \in \mathbb{R}^n \mid x_i \leq y_i \leq \bar{x}_i, \forall i = 1, \dots, n\}. \quad (2)$$

When the bounds are important, we denote an interval $[x]$ by $[\underline{x}, \bar{x}]$, where \underline{x} and \bar{x} are the infimum and supremum, respectively, of $[x]$. Let the operations \inf and \sup return the infimum and supremum of an interval:

$$\inf([x]) = \underline{x} \quad (3)$$

$$\sup([x]) = \bar{x}. \quad (4)$$

Let \mathbb{IR}^n be the set of all real-valued n -dimensional interval vectors.

The Minkowski sum and difference of $[x]$ and $[y]$ are

$$[x] \oplus [y] = [\underline{x} + \underline{y}, \bar{x} + \bar{y}], \quad (5)$$

$$[x] \ominus [y] = [\underline{x} - \bar{y}, \bar{x} - \underline{y}]. \quad (6)$$

The product of $[x]$ and $[y]$ is

$$[x][y] = [\min(\underline{xy}, \underline{x}\bar{y}, \bar{x}\underline{y}, \bar{x}\bar{y}), \max(\underline{xy}, \underline{x}\bar{y}, \bar{x}\underline{y}, \bar{x}\bar{y})]. \quad (7)$$

Given a scalar interval $[a]$ or interval matrix $[Y]$ multiplied by an interval matrix $[X]$, the element in the i^{th} row and j^{th} column of the product is

$$([a][X])_{ij} = [a][X]_{ij}, \quad (8)$$

$$([X][Y])_{ij} = \bigoplus_{k=1}^n ([X]_{ik}[Y]_{kj}), \quad (9)$$

where n is the number of columns of $[X]$ and number of rows of $[Y]$. Lastly, given two interval vectors $[x], [y] \subset \mathbb{R}^3$, their cross product is

$$[x] \otimes [y] = [x]^\times [y], \quad (10)$$

where $[x]^\times$ is the skew-symmetric matrix representation of $[x]$ as in (1) (i.e., a matrix with interval entries).

C. Zonotopes

Because multidimensional intervals can only describe hyperrectangles, they may be overly conservative when outer approximating more general shapes. To build a tighter outer-approximative representation of multidimensional sets, we use zonotopes. A *zonotope* $Z \subset \mathbb{R}^n$ is a convex, centrally-symmetric polytope defined by a *center* $g_0 \in \mathbb{R}^n$ and *generators* $g_i \in \mathbb{R}^n$:

$$Z = \left\{ z \in \mathbb{R}^n \mid z = g_0 + \sum_{i=1}^{n_g} g_i \beta_i, \beta_i \in [-1, 1] \right\} \quad (11)$$

where there are $n_g \in \mathbb{N}$ generators.

Note that the Minkowski sum of a pair of zonotopes is a zonotope [46]. Furthermore, a zonotope can be overapproximated by an interval:

Lemma 1 (Zonotope Interval Overapproximation). *Let $Z \subset \mathbb{R}^n$ with center g_0 and n_g generators g_i . Then, $Z \subseteq [g_0 - \sum_{i=1}^{n_g} |g_i|, g_0 + \sum_{i=1}^{n_g} |g_i|]$.*

Proof. This follows from the definition in (11). \square

Throughout this paper, we often need to represent sets of matrices (e.g., to represent an uncertain inertia matrix). One way to do this is to use a matrix zonotope $M \subset \mathbb{R}^{n \times m}$, which is a zonotope whose center $G_0 \in \mathbb{R}^{n \times m}$ and generators G_i are matrices:

$$M = \left\{ A \in \mathbb{R}^{n \times m} \mid A = G_0 + \sum_{i=1}^{n_g} G_i \beta_i, \beta_i \in [-1, 1] \right\}. \quad (12)$$

Our previous work [3] used matrix zonotopes to represent sets of rotations, and zonotopes to represent the volume of a link. Thus, to represent the swept volume corresponding to uncertain rotations, it was necessary to take the product of matrix zonotopes and zonotopes. To define this product, consider a

matrix zonotope M and zonotope Z of appropriate sizes. In particular, let M have n_g generators G_i with indeterminates β_i , and Z have n_h generators h_j with indeterminates λ_j . Then,

$$MZ = \{ z \in \mathbb{R}^n \mid z = Ay, A \in M, y \in Z \} \quad (13)$$

$$= \left\{ z \in \mathbb{R}^n \mid z = G_0 g_0 + \sum_{j=1}^{n_h} G_0 g_j \lambda_j + \sum_{i=1}^{n_g} G_i g_0 \beta_i + \sum_{i=1}^{n_g} \sum_{j=1}^{n_h} G_i g_j \beta_i \lambda_j, \beta_i \in [-1, 1], \lambda_j \in [-1, 1] \right\} \quad (14)$$

However, the result is no longer a zonotope due to the products of indeterminates $\beta_i \lambda_j$. This motivates the need for a more complex set representation called polynomial zonotopes [2].

D. Polynomial Zonotopes

We present an overview of the necessary definitions and operations of polynomial zonotopes (PZs) in this subsection. A thorough introduction is available [2].

To ease the introduction of polynomial zonotopes, we begin by defining zonotopes using an alternative notation. Let the zonotope Z have center g_0 , n_g generators g_i , and indeterminates β_i . We introduce an indeterminate vector $x \in [-1, 1]^{n_g}$ such that the i^{th} element of x is the indeterminate β_i . Next, we introduce the exponents $\alpha_i \in \mathbb{N}^{n_g}$. Letting $\alpha_1 = [1, 0, \dots, 0]$, $\alpha_2 = [0, 1, 0, \dots, 0]$, ..., $\alpha_{n_g} = [0, 0, \dots, 0, 1]$, we note that $x^{\alpha_1} = x_1, \dots, x^{\alpha_{n_g}} = x_{n_g}$ where the exponentiation is applied element-wise. Then, letting the center g_0 be associated with the exponent $\alpha_0 = [0, 0, \dots, 0]$, we can write Z as

$$Z = \left\{ z \in \mathbb{R}^n \mid z = \sum_{i=0}^{n_g} g_i x^{\alpha_i}, x \in [-1, 1]^{n_g} \right\}. \quad (15)$$

That is, Z is the set of points produced by the polynomial $p(x) = \sum_{i=0}^{n_g} g_i x^{\alpha_i}$ over the domain $x \in [-1, 1]^{n_g}$. Thus, we have a *polynomial zonotope*, a set representation which includes zonotopes as a subset. Though in (15) we defined a zonotope where each α_i has only one nonzero element, note polynomial zonotopes may employ exponents $\alpha_i \in \mathbb{N}^{n_g}$ that are arbitrary.

Definition 2 (Polynomial Zonotope). *A polynomial zonotope $\mathbf{P} \subset \mathbb{R}^n$ is given by its generators $g_i \in \mathbb{R}^n$ (of which there are n_g), exponents $\alpha_i \in \mathbb{N}^{n_g}$, and indeterminates $x \in [-1, 1]^{n_g}$ as*

$$\mathbf{P} = \mathcal{PZ}(g_i, \alpha_i, x) = \left\{ z \in \mathbb{R}^n \mid z = \sum_{i=0}^{n_g} g_i x^{\alpha_i}, x \in [-1, 1]^{n_g} \right\}. \quad (16)$$

We refer to x^{α_i} as a monomial. A term $g_i x^{\alpha_i}$ is produced by multiplying a monomial by the associated generator g_i .

Throughout this document, we exclusively use bold symbols to denote polynomial zonotopes. Next, we introduce several useful operations on polynomial zonotopes: interval conversions, set addition and multiplication, slicing, computing bounds, order reduction, and set-valued function evaluation.

1) *Intervals Conversion*: Similar to zonotopes, intervals can also be written as polynomial zonotopes. Consider the interval $[z] = [\underline{z}, \bar{z}] \subset \mathbb{R}^n$. We can convert $[z]$ to a polynomial zonotope \mathbf{z} using

$$\mathbf{z} = \frac{\bar{z} + \underline{z}}{2} + \sum_{i=1}^n \frac{\bar{z}_i - \underline{z}_i}{2} x_i, \quad (17)$$

where $x \in [-1, 1]^n$ is the indeterminate vector.

2) *Set Addition and Multiplication*: The Minkowski Sum of two polynomial zonotopes $\mathbf{P}_1 \subset \mathbb{R}^n = \mathcal{PZ}(g_i, \alpha_i, x)$ and $\mathbf{P}_2 \subset \mathbb{R}^n = \mathcal{PZ}(h_j, \beta_j, y)$ follows from polynomial addition:

$$\mathbf{P}_1 \oplus \mathbf{P}_2 = \{z \in \mathbb{R}^n \mid z = p_1 + p_2, p_1 \in \mathbf{P}_1, p_2 \in \mathbf{P}_2\} \quad (18)$$

$$= \left\{ z \in \mathbb{R}^n \mid z = \sum_{i=0}^{n_g} g_i x^{\alpha_i} + \sum_{j=0}^{n_h} h_j y^{\beta_j} \right\}. \quad (19)$$

Similarly, we may write the matrix product of two polynomial zonotopes \mathbf{P}_1 and \mathbf{P}_2 when the sizes are compatible (i.e., elements in \mathbf{P}_1 have the same number of columns as elements of \mathbf{P}_2 have rows). Letting $\mathbf{P}_1 \subset \mathbb{R}^{n \times m}$ and $\mathbf{P}_2 \subset \mathbb{R}^{m \times k}$, we obtain $\mathbf{P}_1 \mathbf{P}_2 \subset \mathbb{R}^{n \times k}$:

$$\mathbf{P}_1 \mathbf{P}_2 = \left\{ z \in \mathbb{R}^{n \times k} \mid z = p_1 p_2, p_1 \in \mathbf{P}_1, p_2 \in \mathbf{P}_2 \right\} \quad (20)$$

$$= \left\{ z \in \mathbb{R}^{n \times k} \mid z = \sum_{i=0}^{n_g} g_i \left(\sum_{j=0}^q h_j y^{\beta_j} \right) x^{\alpha_i} \right\}. \quad (21)$$

When $\mathbf{P}_1 \subset \mathbb{R}^{n \times n}$ is square, exponentiation \mathbf{P}_1^m may be performed by multiplying \mathbf{P}_1 by itself m times.

Furthermore, if $\mathbf{P}_1 \subset \mathbb{R}^3$ and $\mathbf{P}_2 \subset \mathbb{R}^3$, we implement a set-based cross product as matrix multiplication. We create $\mathbf{P}_1^\times \subset \mathbb{R}^{3 \times 3}$ as

$$\mathbf{P}_1^\times = \left\{ A \in \mathbb{R}^{3 \times 3} \mid A = \sum_{i=0}^{n_g} \begin{bmatrix} 0 & -g_{i,3} & g_{i,2} \\ g_{i,3} & 0 & -g_{i,1} \\ -g_{i,2} & g_{i,1} & 0 \end{bmatrix} x^{\alpha_i} \right\} \quad (22)$$

where $g_{i,j}$ refers to the j^{th} element of g_i . Then, the set-based cross product $\mathbf{P}_1 \otimes \mathbf{P}_2 = \mathbf{P}_1^\times \mathbf{P}_2$ is well-defined. We briefly note that the addition, multiplication and cross product of a polynomial zonotope with a constant vector or matrix is well-defined if the constant is appropriately sized. In this case, one constructs a polynomial zonotope with that constant vector or matrix as the center g_0 and no other generators, and applies the definitions above.

Both Minkowski summation and multiplication of polynomial zonotopes can be complicated by the fact that \mathbf{P}_1 and \mathbf{P}_2 may share indeterminates. For instance, in the examples above, the i -th element of x and the j -th element of y may represent the same indeterminate. In practice, polynomial zonotopes can be brought to a *common representation* by only considering unique indeterminates before applying the operations above, as discussed in [2, Sec. II.a.1].

3) *Slicing*: One desirable property of polynomial zonotopes is the ability to obtain subsets by plugging in values of known indeterminates. For example, say a polynomial zonotope \mathbf{P} represented a set of possible positions of a robot arm operating near an obstacle. It may be beneficial to know whether a particular choice of \mathbf{P} 's indeterminates yields a subset of positions that could collide with the obstacle. To this end, we introduce the operation of "slicing" a polynomial zonotope

$\mathbf{P} = \mathcal{PZ}(g_i, \alpha_i, x)$ by evaluating an element of the indeterminate x . Given the j^{th} indeterminate x_j and a value $\sigma \in [-1, 1]$, slicing yields a subset of \mathbf{P} by plugging σ into the specified element x_j :

$$\text{slice}(\mathbf{P}, x_j, \sigma) \subset \mathbf{P} = \left\{ z \in \mathbf{P} \mid z = \sum_{i=0}^{n_g} g_i x^{\alpha_i}, x_j = \sigma \right\}. \quad (23)$$

4) *Bounding a PZ*: Later in this document, we require a means to bound the elements of a polynomial zonotope. In particular, we define the \sup and \inf operations which return these upper and lower bounds, respectively, by taking the absolute values of generators. For $\mathbf{P} \subseteq \mathbb{R}^n$ with center g_0 and generators g_i ,

$$\sup(\mathbf{P}) = g_0 + \sum_{i=1}^{n_g} |g_i|, \quad (24)$$

$$\inf(\mathbf{P}) = g_0 - \sum_{i=1}^{n_g} |g_i|. \quad (25)$$

Note that for any $z \in \mathbf{P}$, $\sup(\mathbf{P}) \geq z$ and $\inf(\mathbf{P}) \leq z$, where the inequalities are taken element-wise. These bounds may not be tight, because possible dependencies between indeterminates are not accounted for, but they are quick to compute.

5) *Set-Valued Function Evaluation*: Though we have defined several basic operations like addition and multiplication above, it may be desirable to use polynomial zonotopes as inputs to more complicated functions. One can overapproximate any analytic function evaluated on a polynomial zonotope using a Taylor expansion, which itself can be represented as a polynomial zonotope [47, Sec 4.1][2, Prop. 13]. Consider an analytic function $f: \mathbb{R} \rightarrow \mathbb{R}$ and $\mathbf{P}_1 = \mathcal{PZ}(g_i, \alpha_i, x)$, with each $g_i \in \mathbb{R}$. Then,

$$f(\mathbf{P}_1) = \{y \in \mathbb{R} \mid y = f(z), z \in \mathbf{P}_1\}. \quad (26)$$

We generate \mathbf{P}_2 such that $f(\mathbf{P}_1) \subseteq \mathbf{P}_2$ using a Taylor expansion of degree $d \in \mathbb{N}$, where the error incurred from the finite approximation is overapproximated using a Lagrange remainder. The method follows the Taylor expansion found in the reachability algorithm in [2], which builds on previous work on conservative polynomialization found in [47]. Recall that the Taylor expansion about a point $c \in \mathbb{R}$ is

$$f(z) = \sum_{n=0}^{\infty} \frac{f^{(n)}(c)}{n!} (z-c)^n, \quad (27)$$

where $f^{(n)}$ is the n^{th} derivative of f . Note that the error incurred by a finite Taylor expansion can be bounded using the Lagrange remainder r [48, p. 7.7]:

$$|f(z) - \sum_{n=0}^d \frac{f^{(n)}(c)}{n!} (z-c)^n| \leq r, \quad (28)$$

where r is given by

$$r = \frac{M |z-c|^{d+1}}{(d+1)!}, \quad (29)$$

$$M = \max_{\delta \in [c, z]} (|f^{(d+1)}(\delta)|). \quad (30)$$

TABLE I
Summary of polynomial zonotope operations.

Operation	Computation
$[z] \rightarrow \mathbf{z}$ (Interval Conversion) (17)	Exact
$\mathbf{Z} \rightarrow \mathbf{Z}$ (Zonotope Conversion) (15)	Exact
$\mathbf{P}_1 \oplus \mathbf{P}_2$ (Minkowski Sum) (19)	Exact
$\mathbf{P}_1 \mathbf{P}_2$ (Set Multiplication) (21)	Exact
\mathbf{P}^n (Exponentiation)	Exact
$\mathbf{P}_1 \otimes \mathbf{P}_2$ (Set Cross Product) (22)	Exact
$\text{slice}(\mathbf{P}, x_j, \sigma)$ (23)	Exact
$\sup(\mathbf{P})$ (24) and $\inf(\mathbf{P})$ (25)	Overapproximative
$f(\mathbf{P}_1) \subseteq \mathbf{P}_2$ (Taylor expansion) (32)	Overapproximative

For a polynomial zonotope, the infinite dimensional Taylor expansion is given by

$$f(\mathbf{P}_1) = \sum_{n=0}^{\infty} \frac{f^{(n)}(c)}{n!} (\mathbf{P}_1 - c)^n \quad (31)$$

In practice, only a finite Taylor expansion of degree $d \in \mathbb{N}$ can be computed. Letting $c = g_0$ (i.e., the center of \mathbf{P}_1), and noting that $(z - c) = \sum_{i=1}^{n_g} g_i x^{\alpha_i}$ for $z \in \mathbf{P}_1$, we write

$$\mathbf{P}_2 := \left\{ z \in \mathbb{R} \mid z \in \sum_{n=0}^d \left(\frac{f^{(n)}(g_0)}{n!} \left(\sum_{i=1}^{n_g} g_i x^{\alpha_i} \right)^n \right) \oplus [r] \right\} \quad (32)$$

and the Lagrange remainder $[r]$ can be computed using interval arithmetic as

$$[r] = \frac{[M][(\mathbf{P}_1 - c)^{d+1}]}{(d+1)!}, \quad (33)$$

$$[M] = f^{(d+1)}([\mathbf{P}_1]) \quad (34)$$

where $[(\mathbf{P}_1 - c)^{d+1}] = [\inf((\mathbf{P}_1 - c)^{d+1}), \sup((\mathbf{P}_1 - c)^{d+1})]$ is an overapproximation of $(\mathbf{P}_1 - c)^{d+1}$. Note that \mathbf{P}_2 can be expressed as a polynomial zonotope because all terms in the summation are polynomials of x , and the interval $[r]$ can be expressed as a polynomial zonotope as in (17). Just as we denote polynomial zonotopes using bold symbols, we denote the polynomial zonotope overapproximation of a function evaluated on a zonotope using bold symbols (i.e., $\mathbf{f}(\mathbf{P}_1)$ is the polynomial zonotope over approximation of f applied to \mathbf{P}).

Note the usual order of operations for addition, multiplication and exponentiation apply for polynomial zonotope operations as well. Table I summarizes these operations. Note as described in the table these operations can either be computed exactly or in an overapproximative fashion using polynomial zonotopes.

IV. ARM AND ENVIRONMENT

The goal of this work is to plan guaranteed-safe trajectories for serial manipulators with uncertain inertial properties in real time. This section introduces the robot arm's kinematics and dynamics, and defines the environment and obstacles.

A. Robotic Manipulator Model

Given an n_q -dimensional serial robotic manipulator with configuration space \mathcal{Q} and a compact time interval $T \subset \mathbb{R}$ we define a trajectory for the configuration as $q: T \rightarrow \mathcal{Q} \subset \mathbb{R}^{n_q}$.

The velocity of the robot is $\dot{q}: T \rightarrow \mathbb{R}^{n_q}$. Let $N_q = \{1, \dots, n_q\}$. We make the following assumptions about the structure of the robot model:

Assumption 3 (Workspace and Configuration Space). *The robot operates in a three dimensional workspace, which we denote $W \subset \mathbb{R}^3$. The robot is composed of only revolute joints, where the j^{th} joint actuates the robot's j^{th} link. The robot's j^{th} joint has position and velocity limits given by $q_j(t) \in [q_{j,\text{lim}}^-, q_{j,\text{lim}}^+]$ and $\dot{q}_j(t) \in [\dot{q}_{j,\text{lim}}^-, \dot{q}_{j,\text{lim}}^+]$ for all $t \in T$, respectively. During online operation, the robot has encoders that allow it to measure its joint positions and velocities. Finally, the robot is fully actuated, where the robot's input $u: T \rightarrow \mathbb{R}^{n_q}$ has limits that are given by $u_j(t) \in [u_{j,\text{lim}}^-, u_{j,\text{lim}}^+]$ for all $t \in T$ and $j \in N_q$.*

Note that we make the one-joint-per-link assumption with no loss of generality because joints with multiple degrees of freedom (e.g., spherical joints) may be represented in this framework using links with zero length. In addition, this work can be extended to robots with prismatic joints by straightforward extensions to the RNEA algorithms presented in Sec. VIII.

1) *Arm Kinematics*: Next, we introduce the robot's kinematics. Suppose there exists a fixed inertial reference frame, which we call the *world* frame. In addition suppose there exists a *base* frame, which we denote the 0^{th} frame, that indicates the origin of the robot's kinematic chain. We assume that the j^{th} reference frame $\{\hat{x}_j, \hat{y}_j, \hat{z}_j\}$ is attached to the robot's j^{th} revolute joint, and that $\hat{z}_j = [0, 0, 1]^T$ corresponds to the j^{th} joint's axis of rotation. Then for a configuration at a particular time, $q(t)$, the position and orientation of frame j with respect to frame $j-1$ can be expressed using the homogeneous transformation matrix $H_j^{j-1}(q_j(t))$ [49, Ch. 2] defined by

$$H_j^{j-1}(q_j(t)) = \begin{bmatrix} R_j^{j-1}(q_j(t)) & p_j^{j-1} \\ 0 & 1 \end{bmatrix}, \quad (35)$$

where $R_j^{j-1}(q_j(t))$ is a configuration-dependent rotation matrix and p_j^{j-1} is the fixed translation vector from frame $j-1$ to frame j . Note that we use the non-standard notation H_j^{j-1} to avoid confusion with other symbols denoting time.

With these definitions, we can express the forward kinematics of the robot. Let $\text{FK}_j: \mathcal{Q} \rightarrow \mathbb{R}^{4 \times 4}$ map the robot's configuration to the position and orientation of the j^{th} joint in the world frame:

$$\text{FK}_j(q(t)) = \prod_{l=1}^j H_l^{l-1}(q_l(t)) = \begin{bmatrix} R_j(q(t)) & p_j(q(t)) \\ 0 & 1 \end{bmatrix}, \quad (36)$$

where

$$R_j(q(t)) := R_j^0(q(t)) = \prod_{l=1}^j R_l^{l-1}(q_l(t)) \quad (37)$$

and

$$p_j(q(t)) = \sum_{l=1}^j R_l(q(t)) p_l^{l-1}. \quad (38)$$

2) *Arm Occupancy*: An arm's kinematics can be used to describe the volume occupied by the arm in the workspace. Let $L_j \subset \mathbb{R}^3$ denote the volume occupied by the j^{th} link with respect to the j^{th} reference frame. Then the map $\text{FO}_j : Q \rightarrow \text{pow}(W)$ gives the forward occupancy of link j :

$$\text{FO}_j(q(t)) = p_j(q(t)) \oplus R_j(q(t))L_j, \quad (39)$$

where the first expression gives the position of joint j and the second gives the rotated volume of link j . The function $\text{FO} : Q \rightarrow \text{pow}(W)$ then gives the volume occupied by the entire arm in the workspace:

$$\text{FO}(q(t)) = \bigcup_{j=1}^{n_q} \text{FO}_j(q(t)) \subset W. \quad (40)$$

3) *Arm Dynamics*: We assume the robot is composed of n_q rigid links with inertial parameters given by the vector

$$\Delta = (m_1, \dots, m_{n_q}, c_{x,1}, \dots, c_{z,n_q}, I_{xx,1}, \dots, I_{zz,n_q}) \quad (41)$$

where m_j , $c_j = (c_{x,j}, c_{y,j}, c_{z,j})$, and $(I_{xx,j}, \dots, I_{zz,j})$ represent the mass, center of mass, and inertia tensor of the j^{th} link, respectively. The dynamics are represented by the standard manipulator equations [49]:

$$M(q(t), \Delta) \ddot{q}(t) + C(q(t), \dot{q}(t), \Delta) \dot{q}(t) + G(q(t), \Delta) = u(t) \quad (42)$$

where $M(q(t), \Delta) \in \mathbb{R}^{n_q \times n_q}$ is the positive definite inertia matrix, $C(q(t), \dot{q}(t), \Delta)$ is the Coriolis matrix, $G(q(t), \Delta)$ is the gravity vector, and $u(t)$ is the input torque all at time t . Note, for simplicity, we do not explicitly model friction, but it can be incorporated in $G(q(t), \Delta)$ [37], [39].

We make the following assumptions about the robot's inertial parameters:

Assumption 4 (Inertial Parameter Bounds). *The model structure (i.e., number of joints, sizes of links, etc.) of the robot is known, but its true inertial parameters Δ are unknown. The uncertainty in each inertial parameter is known and given by the interval vector*

$$[\Delta] = ([m_1], \dots, [m_{n_q}], [c_{x,1}], \dots, [c_{z,n_q}], [I_{xx,1}], \dots, [I_{zz,n_q}])^\top \quad (43)$$

where $[m_j] \subset \mathbb{R}$, $[c_j] \subset \mathbb{R}^3$, and $[I_j] \subset \mathbb{R}^{3 \times 3}$ represent the uncertainties in the mass, center of mass, and inertia tensor of the j^{th} link, respectively. The true parameters lie in this interval, i.e., $\Delta \in [\Delta]$. Any inertia tensor drawn from $[I_j]$ must be positive semidefinite. In addition, if we let $[\Delta]_j$ denote the j^{th} component of $[\Delta]$, then $\inf([\Delta]_j) > -\infty$ and $\sup([\Delta]_j) < \infty$ for all j . Finally, there exists a nominal vector of inertial parameters $\Delta_0 \in [\Delta]$ that serves as an estimate of the true parameters of the system.

Note, we do not assume that Δ_0 is equal to the true parameters of the system or even a good estimate to the true parameters.

B. Environment

Next, we speak about obstacles and the start and goal configurations of the robot.

1) *Obstacles*: We begin by defining and making a few assumptions about obstacles:

Assumption 5 (Obstacles). *The transformation between the world frame of the workspace and the base frame of the robot is assumed to be known, and obstacles are expressed in the base frame of the robot. At any time, the number of obstacles $n_\mathcal{O} \in \mathbb{N}$ in the scene is finite ($n_\mathcal{O} < \infty$). Let \mathcal{O} be the set of all obstacles $\{O_1, O_2, \dots, O_{n_\mathcal{O}}\}$. Each obstacle is convex, bounded, and static with respect to time. The arm has access to a zonotope overapproximation of each obstacle's volume in workspace.*

We say that the arm is *in collision* with an obstacle if $\text{FO}_j(q(t)) \cap O_i \neq \emptyset$ for any $j \in N_q$ or $i \in \{1, \dots, n_\mathcal{O}\}$. Note that this work is concerned with planning and control around obstacles, not perception of obstacles. A convex, bounded object can always be overapproximated as a zonotope [46]. In addition, if one is given a non-convex bounded obstacle, then one can outerapproximate that obstacle by computing its convex hull. Dynamic obstacles may also be considered within the ARMOUR framework by introducing a more general notion of safety [50, Definition 11], but we omit this case in this paper to ease exposition. Next, note that we have assumed for convenience that the robot is able to sense all obstacles workspace. However, in practice, one could assume that the robot has a finite sensing horizon in which it is able to sense obstacles. In this instance, one could extend the results regarding the collision free behavior of ARMOUR by applying Theorem 39 in [6]. Finally, if a portion of the scene is occluded then one can treat that portion of the scene as an obstacle.

2) *Task Specification*: We define the arm's task in terms of start and goal configurations:

Definition 6 (Start and Goal Configurations). *The robot begins from rest from the known starting configuration q_{start} . It has zero initial velocity and zero initial acceleration. ARMOUR attempts to find and execute a sequence of safe trajectories from q_{start} to a user-specified goal configuration, q_{goal} .*

We note that an end-effector goal position in workspace may be specified instead of the configuration q_{goal} if desired. We omit this case for simplicity, as it only affects ARMOUR's user-specified cost function in Sec. V.

V. PROPOSED METHOD OVERVIEW

This section provides a high-level overview of ARMOUR. Our objective is to plan safe trajectories in a receding horizon fashion that reach a goal configuration $q_{\text{goal}} \in Q$. To accomplish this goal, ARMOUR optimizes over a space of possible desired trajectories. As described in Section VI, these desired trajectories are chosen from a prespecified continuum of trajectories, with each uniquely determined by a *trajectory parameter*, $k \in K$. During each planning iteration, ARMOUR selects a specific trajectory parameter that can be followed without collisions despite tracking error and model uncertainty. At the same time, these trajectories are guaranteed to satisfy joint and input limits. To ensure that ARMOUR is able to plan in real-time, each desired trajectory is followed while the

robot constructs the next desired trajectory for the subsequent step.

Next, we give overviews of the feedback controller, timing of planning, and trajectory optimization in more detail.

A. Feedback Controller

As is described in Sec. VII, one can associate a feedback control input over a compact time interval $T = [0, t_f] \subset \mathbb{R}$ with each trajectory parameter $k \in K$. This feedback control input can be a function of the nominal inertial parameters, Δ_0 , the interval inertial parameters $[\Delta]$, and the state of the robot; however, it cannot be a function of the true inertial parameters of the robot because these are not assumed to be known. Applying this control input to the arm generates an associated trajectory of the arm. Note that this position and velocity trajectory is a function of the true inertial parameters of the robot. We denote the position and velocity trajectories at time $t \in T$ under trajectory $k \in K$ under the true inertia model parameters $\Delta \in [\Delta]$ by $q(t; k, \Delta)$ and $\dot{q}(t; k, \Delta)$, respectively. To simplify notation, in this section, we denote the feedback control input at time $t \in T$ under trajectory $k \in K$ by $u(t; k)$.

Remark 7 (Controller Dependency Notation). *In the remainder of the paper, the control input is allowed to be a function of the nominal inertial parameters, Δ_0 , the interval inertial parameters, $[\Delta]$, the state of the system, and the trajectory parameter. In particular, although we have suppressed the dependence for ease of reading, we stress that the control input is a function of the state of the robot arm, which is a function of the (unknown) true inertial parameters.*

B. Timing

Because ARMOUR performs receding horizon planning, we assume without loss of generality that the control input and trajectory begin at time $t = 0$ and end at a fixed time t_f . To ensure real-time operation, we require that ARMOUR identify a new trajectory parameter within a fixed planning time of t_p seconds, where $t_p < t_f$. Thus ARMOUR has limited planning time and must select a new trajectory parameter before completing its tracking of the previously identified desired trajectory. If no new trajectory parameter is found in time, ARMOUR defaults to a braking maneuver that brings the robot to a stop at time $t = t_f$. As is described in Sec. VI, we require each desired trajectory to contain such a maneuver, which was verified as safe in the previous planning iteration.

C. Online Trajectory Optimization

During each receding-horizon planning iteration, ARMOUR generates a trajectory by solving a tractable representation to the following nonlinear optimization:

$$\min_{k \in K} \text{cost}(k) \quad (44)$$

$$q_j(t; k, \Delta) \in [q_{j,\text{lim}}^-, q_{j,\text{lim}}^+] \quad \forall t \in T, \Delta \in [\Delta], j \in N_q \quad (45)$$

$$\dot{q}_j(t; k, \Delta) \in [\dot{q}_{j,\text{lim}}^-, \dot{q}_{j,\text{lim}}^+] \quad \forall t \in T, \Delta \in [\Delta], j \in N_q \quad (46)$$

$$u_j(t; k) \in [u_{j,\text{lim}}^-, u_{j,\text{lim}}^+] \quad \forall t \in T, \Delta \in [\Delta], j \in N_q \quad (47)$$

$$\text{FO}_j(q(t; k, \Delta)) \cap \mathcal{O} = \emptyset \quad \forall t \in T, \Delta \in [\Delta], j \in N_q \quad (48)$$

The cost function (44) specifies a user-defined objective, such as bringing the robot close to some desired goal. Each of the constraints guarantee the safety of any feasible trajectory parameter as we describe next. First, the trajectory must be executable by the robot. This means the trajectory must not violate the robot's joint position (45), velocity (46), or input (47) limits. These constraints must be satisfied for each joint over the entire planning horizon despite model uncertainty. Finally, the robot must not collide with any obstacles in the environment (48).

Implementing a real-time optimization algorithm to solve this problem is challenging for several reasons. First, the dynamics of the robot are nonlinear and constructing an explicit solution to them is intractable. Second, the constraints associated with obstacle avoidance are non-convex. Finally, note that the constraints must be satisfied for all time t in an uncountable set T . To address these three challenges, Section VIII proposes a method to generate tight overapproximations to the trajectories and constraints that are differentiable and enable the application of fast optimization techniques.

VI. TRAJECTORY DESIGN

At runtime, ARMOUR computes safe trajectories in a receding-horizon manner by solving an optimization program over parameterized trajectories at each planning iteration. This section describes the parameterized trajectories.

In each planning iteration, ARMOUR chooses a desired trajectory to be followed by the robot. These trajectories are chosen from a pre-specified continuum of trajectories, with each uniquely determined by a trajectory parameter $k \in K$. The set $K \subset \mathbb{R}^{n_k}$, $n_k \in \mathbb{N}$, is compact and represents a user-designed continuum of trajectories. In general, K can be designed to include trajectories designed for a wide variety of tasks and robot morphologies [3], [6], [51], [52], as long as each trajectory satisfies the following properties.

Definition 8 (Trajectory Parameters). *For each $k \in K$, a desired trajectory is an analytic function $q_d(\cdot; k) : T \rightarrow Q$ that satisfies the following properties:*

- I. *The trajectory starts at a specified initial condition $(q_{d_0}, \dot{q}_{d_0}, \ddot{q}_{d_0})$, so that $q_d(0; k) = q_{d_0}$, $\dot{q}_d(0; k) = \dot{q}_{d_0}$, and $\ddot{q}_d(0; k) = \ddot{q}_{d_0}$.*
- II. *$\dot{q}_d(t_f; k) = 0$ and $\ddot{q}_d(t_f; k) = 0$ (i.e., each trajectory brakes to a stop, and at the final time has zero velocity and acceleration).*
- III. *$\ddot{q}_d(\cdot; k)$ is Lipschitz continuous and bounded.*

The first property allows for desired trajectories to be generated online. In particular, recall that ARMOUR performs real-time receding horizon planning by executing a desired trajectory computed at a previous planning iteration while constructing a desired trajectory for the subsequent time interval. The first property allows desired trajectories that are generated by ARMOUR to begin from the appropriate future initial condition of the robot. The second property ensures that a fail safe braking maneuver is always available. The third property ensures that desired position, velocity, and acceleration trajectories for the tracking controller are sufficiently continuous.

VII. CONTROLLER DESIGN

This section describes a robust passivity-based controller that is used to follow the desired trajectories described in the previous section. The controller conservatively handles uncertainty in the manipulator's dynamics stemming from uncertain inertial parameters, and provides a bound on the worst-case tracking error. This tracking error bound is critical to our planning algorithm because it allows us to account for the worst-case tracking performance when following any desired trajectory. Importantly, we show via experiments in Section X that this robust approach is not overly conservative. We use this bound to develop obstacle avoidance and torque limit constraints in Section VIII which are guaranteed to be satisfied when tracking a feasible desired trajectory.

The robust passivity-based controller is a feedback control input that is a function of a desired trajectory parameter. Recall that in Section V, we denote the control input at time $t \in T$ under trajectory $k \in K$ by $u(t; k)$ even though it can also be a function of the nominal inertial parameters, Δ_0 , the interval inertial parameters, $[\Delta]$, and the state of the system. Because this section focuses on proving several important properties regarding the continuity of the controller, we are more deliberate in describing the controller's dependencies. Note that all desired and actual trajectories of the robot depend on the trajectory parameter $k \in K$; however, to avoid overburdening the reader, and because it is clear in context, we drop the dependence of the trajectory on k .

To begin formulating the controller, we begin by defining a *total feedback trajectory*, q_A , that is made up of the robot trajectory and the desired trajectory and is defined as:

$$q_A(t) = [q(t)^\top \quad \dot{q}(t)^\top \quad q_d(t)^\top \quad \dot{q}_d(t)^\top \quad \ddot{q}_d(t)^\top]^\top \quad (49)$$

at time t . Using $q_A(t)$, we can define a *modified desired velocity trajectory*, \dot{q}_a , and *modified desired acceleration trajectory*, \ddot{q}_a as:

$$\begin{aligned} \dot{q}_a(t) &= \dot{q}_d(t) + K_r e(t), \quad e(t) = q_d(t) - q(t) \\ \ddot{q}_a(t) &= \ddot{q}_d(t) + K_r \dot{e}(t), \quad \dot{e}(t) = \dot{q}_d(t) - \dot{q}(t) \end{aligned} \quad (50)$$

where the gain matrix K_r is a diagonal positive definite matrix. Note again that these trajectories do depend on the trajectory parameter $k \in K$; however, we have dropped this dependence for ease of reading in the remainder of the discussion.

The robust passivity-based control input at time $t \in T$ is $u(q_A(t), \Delta_0, [\Delta]) \in \mathbb{R}^{n_q}$, which is composed of a passivity-based nominal input $\tau(q_A(t), \Delta_0) \in \mathbb{R}^{n_q}$, as well as a robust input $v(q_A(t), \Delta_0, [\Delta]) \in \mathbb{R}^{n_q}$:

$$u(q_A(t), \Delta_0, [\Delta]) = \tau(q_A(t), \Delta_0) - v(q_A(t), \Delta_0, [\Delta]). \quad (51)$$

This decomposition is similar to the one proposed in [37], [53]. The justification for this decomposition is that the nominal control input is unable to perfectly execute the desired trajectory because of a possible mismatch between the nominal inertial parameters Δ_0 and the true parameters Δ . Thus, v is introduced as an additional term to guarantee robustness by compensating for the worst possible disturbances stemming from this mismatch in inertial parameters. Despite the similarities to the decomposition proposed in [37], [53], note that

our formulation of v is distinct and significantly improves upon prior approaches by providing the same tracking error bound while requiring a smaller bound on the robust input v , as described in Appendix F. We describe how to construct τ in the next subsection, then our formulation of v in the following subsection, and conclude this section by describing how to compute τ and v .

A. Nominal and Robust Controllers

Per Assumption 4, there exists a nominal model of the robot's dynamics given by inertial parameters Δ_0 . Similar to [53, (4)], our nominal control approach stems from passivity-based control, with the nominal control input given by

$$\tau(q_A(t), \Delta_0) = M(q(t), \Delta_0) \ddot{q}_a(t) + C(q(t), \dot{q}(t), \Delta_0) \dot{q}_a(t) + G(q(t), \Delta_0). \quad (52)$$

We treat the torques that arise from the possible mismatch between the nominal parameters Δ_0 and the true parameters Δ as a disturbance w , where

$$\begin{aligned} w(q_A(t), \Delta_0, \Delta) &= (M(q(t), \Delta) - M(q(t), \Delta_0)) \ddot{q}_a(t) + \\ &+ (C(q(t), \dot{q}(t), \Delta) - C(q(t), \dot{q}(t), \Delta_0)) \dot{q}_a + \\ &+ G(q(t), \Delta) - G(q(t), \Delta_0). \end{aligned} \quad (53)$$

In practice, w is unknown, but can be bounded by

$$w(q_A(t), \Delta_0, \Delta) \in [w(q_A(t), \Delta_0, [\Delta])], \quad (54)$$

where the right hand side of the previous equation is computed by plugging $[\Delta]$ into (53) in place of Δ and using interval arithmetic. Note, we describe how to compute $[w(q_A(t), \Delta_0, [\Delta])]$ using Algorithm 1 in the next subsection.

To create our controller, we next define a function that measures the worst case disturbance:

Definition 9 (Worst Case Disturbance). *Suppose that we have $\inf([w(q_A(t), \Delta_0, [\Delta])]) = \underline{w}$ and $\sup([w(q_A(t), \Delta_0, [\Delta])]) = \bar{w}$. Then the measure of worst case disturbance is the function $\rho : \mathbb{R}^{n_q} \rightarrow \mathbb{R}^{n_q}$ which is defined as*

$$\rho([w(q_A(t), \Delta_0, [\Delta])]) = \max(|\underline{w}|, |\bar{w}|), \quad (55)$$

where the max operator is applied element-wise.

The absolute value of the disturbance $|w(q_A(t), \Delta_0, \Delta)|$ is always bounded by the worst-case disturbance (55):

Lemma 10 (Disturbance Bound). *For all $q_A(t) \in \mathbb{R}^{6n_q}$ and $\Delta \in [\Delta]$*

$$\rho([w(q_A(t), \Delta_0, [\Delta])]) \geq |w(q_A(t), \Delta_0, \Delta)|, \quad (56)$$

where the inequality is applied element-wise.

Proof. Throughout the proof, we suppress the dependence on $q_A(t)$, Δ , and Δ_0 for convenience. Notice that the true disturbance w is contained in the interval $[w]$ as in (54). Therefore, $|w| \in [0, \max(|\underline{w}|, |\bar{w}|)]$. Next from Def. 9, $\rho([w]) = \max(|\underline{w}|, |\bar{w}|)$, and so $\rho([w]) \geq |w| \forall w \in [w]$. \square

Plugging the control input (51) into the manipulator dynamics (42), and substituting in the form of the nominal input (52) and disturbance (53), one obtains

$$v(q_A(t), \Delta_0, [\Delta]) + w(q_A(t), \Delta_0, \Delta) = M(q(t), \Delta) \dot{r}(t) + C(q(t), \dot{q}(t), \Delta) r(t) \quad (57)$$

where $r(t)$ is the *modified tracking error*

$$\begin{aligned} r(t) &= \dot{e}(t) + K_r e(t) \\ \dot{r}(t) &= \ddot{e}(t) + K_r \dot{e}(t). \end{aligned} \quad (58)$$

Our goal is to obtain a uniform bound on the modified tracking error, $r : T \rightarrow \mathbb{R}^{n_q}$.

To do this, we make the following assumption about the mass matrix $M(q(t), \Delta)$:

Assumption 11 (Mass Matrix Eigenvalue Bound). *Let $\lambda_m(M(q(t), \Delta))$ and $\lambda_M(M(q(t), \Delta))$ be the minimum and maximum eigenvalues of $M(q(t), \Delta)$. There exist finite uniform bounds $\sigma_m > 0$ and $\sigma_M > 0$ on these eigenvalue so that*

$$0 < \sigma_m \leq \lambda_m(M(q(t), \Delta)) \quad (59)$$

$$0 < \lambda_M(M(q(t), \Delta)) \leq \sigma_M \quad (60)$$

holds for all $q(t) \in Q$ and $\Delta \in [\Delta]$.

Using classical analysis arguments, one can prove that if $M(q(t), \Delta)$ is positive definite for all $q(t)$ and Δ , then σ_m is at least equal to zero. However proving that this lower bound is greater than zero does require more explicit structure on $[\Delta]$. Because this is not the emphasis of this paper, we make this assumption and verify that it is satisfied numerically during experiments.

We next state a theorem whose proof can be found in Appendix A that describes how to construct the robust input v in (51) by making use of the worst-case disturbance (55) and the previous assumption to achieve a uniformly bounded tracking error for r .

Theorem 12 (Uniform Tracking Error Bound). *Suppose Assumption 11 is satisfied. Let $V_M > 0$ be a user-specified constant and consider the following candidate Lyapunov function*

$$V(q_A(t), \Delta) = \frac{1}{2} r(t)^\top M(q(t), \Delta) r(t). \quad (61)$$

Let h be a function that is continuous in its first argument such that

$$h(q_A(t), [\Delta]) \leq - \sup_{\Delta^* \in [\Delta]} (V(q_A(t), \Delta^*)) + V_M, \quad (62)$$

for all $q_A(t)$. Let $\alpha : \mathbb{R} \rightarrow \mathbb{R}$ be some extended class \mathcal{K}_∞ function (i.e., $\alpha : \mathbb{R} \rightarrow \mathbb{R}$ is strictly increasing with $\alpha(0) = 0$). Let w_M be any continuous function in its first argument such that

$$w_M(q_A(t), \Delta_0, [\Delta]) \geq \rho([w(q_A(t), \Delta_0, [\Delta])]), \quad (63)$$

for all $q_A(t)$, Δ_0 , and $[\Delta]$, where the inequality is applied element-wise. Finally, suppose that $e(0) = \dot{e}(0) = 0$ and let

$$\varepsilon := \sqrt{\frac{2V_M}{\sigma_m}}. \quad (64)$$

If the robust input is set equal to

$$v(q_A(t), \Delta_0, [\Delta]) = \begin{cases} -\gamma(q_A(t), \Delta_0, [\Delta]) \frac{r(t)}{\|r(t)\|} & \|r(t)\| \neq 0 \\ 0 & \|r(t)\| = 0 \end{cases} \quad (65)$$

with

$$\gamma(q_A(t), \Delta_0, [\Delta]) = \max \left(0, \frac{-\alpha(h(q_A(t), [\Delta]))}{\|r(t)\|} + \frac{|r(t)|^\top w_M(q_A(t), \Delta_0, [\Delta])}{\|r(t)\|} \right), \quad (66)$$

then the modified tracking error trajectories $r : T \rightarrow \mathbb{R}^{n_q}$ are uniformly bounded by

$$\|r(t)\| \leq \varepsilon \quad \forall t \in T \quad (67)$$

when tracking desired trajectories that satisfy Def. 8.

Theorem 12 provides a uniform bound on the tracking error trajectories $r : T \rightarrow \mathbb{R}^{n_q}$. This bound can be used to provide bounds on the position error and velocity error of the robot, which we utilize for planning desired trajectories in Section VIII. The following claim, whose proof can be found in Appendix B, is inspired by [53, Corollary 6] and [54, Proof of Theorem 2.3], but differs from these works because we consider a uniform bound on $r : T \rightarrow \mathbb{R}^{n_q}$ (67) that applies for all T , rather than an ultimate bound that is only valid after some finite time:

Corollary 13 (Tracking Performance). *Suppose Assumption 11 is satisfied and $e(0) = \dot{e}(0) = 0$. If $r : T \rightarrow \mathbb{R}^{n_q}$ is uniformly bounded as in (67), then the controller (51) with robust input (65) reaches any desired tracking performance provided a large enough gain matrix K_r . In particular, letting*

$$\varepsilon_{p,j} := \frac{\varepsilon}{K_{r,j}} \quad \text{and} \quad (68)$$

$$\varepsilon_v := 2\varepsilon, \quad (69)$$

where ε as in (64) and $K_{r,j}$ is the j^{th} element of the diagonal gain matrix K_r , then $|e_j(t)| \leq \varepsilon_{p,j}$ and $|\dot{e}_j(t)| \leq \varepsilon_v$ for all $t \in T$ and $j \in N_q$.

Though theoretically these bounds can be made arbitrarily small, in practice they are limited by the physical capabilities of the robot. Enforcing very small bounds may require large torques, causing input saturation. In Section VIII, we explain how to overapproximate the torques required to track a given desired trajectory including all possible tracking error. We use these overapproximations to design desired trajectories that are guaranteed to be physically realizable on the robot in Section IX.

Before proceeding further, we make one final remark about the validity of these bounds for all time rather than just over $t \in T$.

Remark 14 (Error Bound for All Time). *By Def. 6, the robot starts from configuration q_{start} with zero initial velocity and acceleration. Suppose that the initial condition of the desired trajectory in the first planning iteration matches this (i.e., $q_{d_0} = q_{\text{start}}$, $\dot{q}_{d_0} = 0$, $\ddot{q}_{d_0} = 0$), and that the initial condition of all subsequent desired trajectories match the state of the*

Algorithm 1:

```

 $\{[u_j(t, [\Delta])] : j \in n_q\} = \text{IRNEA}(q_A(t), [\Delta], a_0^0)$ 
1: Compute  $\dot{q}_a(t)$  and  $\ddot{q}_a(t)$  using (50).
2: Initialize base linear acceleration  $a_0^0$ .
3: for  $j = 1 : n_q$  // for each joint
4:    $R_j^{j-1}, p_j^{j-1} \leftarrow H_j^{j-1}(q_j(t))$  as in (35)
5:    $R_{j-1}^j \leftarrow \text{transpose}(R_j^{j-1})$ 
6: end for
7: for  $j = 1 : n_q$  // for each joint (forward recursion)
8:    $\omega_j^j \leftarrow R_{j-1}^j \omega_{j-1}^{j-1} + \dot{q}_j(t) \hat{z}_j$ 
9:    $\omega_{a,j}^j \leftarrow R_{j-1}^j \omega_{a,j-1}^{j-1} + \ddot{q}_{a,j}(t) \hat{z}_j$ 
10:   $\dot{\omega}_j^j \leftarrow R_{j-1}^j \dot{\omega}_{j-1}^{j-1} + ((R_{j-1}^j \omega_{a,j-1}^{j-1}) \times (\dot{q}_j(t) \hat{z}_j)) + \ddot{q}_{a,j}(t) \hat{z}_j$ 
11:   $a_j^j \leftarrow (R_{j-1}^j a_{j-1}^{j-1}) + (\dot{\omega}_j^j \times p_j^{j-1}) + (\omega_j^j \times (\omega_{a,j}^j \times p_j^{j-1}))$ 
12:   $[a_{c,j}^j] \leftarrow a_j^j + (\dot{\omega}_j^j \otimes [c_j^j]) + (\omega_j^j \otimes (\omega_{a,j}^j \otimes [c_j^j]))$ 
13:   $[F_j^j] \leftarrow [m_i][a_{c,j}^j]$ 
14:   $[N_j^j] \leftarrow [I_j^j] \dot{\omega}_j^j \oplus (\omega_{a,j}^j \otimes ([I_j^j] \omega_j^j))$ 
15: end for
16:  $R_{n_q+1}^{n_q} \leftarrow I_{3 \times 3}$ 
17:  $[f_{n_q+1}^{n_q+1}] \leftarrow 0$ 
18:  $[n_{n_q+1}^{n_q+1}] \leftarrow 0$ 
19: for  $j = n_q : -1 : 1$  // for each joint (backward recursion)
20:    $[f_j^j] \leftarrow (R_{j+1}^j [f_{j+1}^{j+1}]) \oplus [F_j^j]$ 
21:    $[n_j^j] \leftarrow (R_{j+1}^j [n_{j+1}^{j+1}]) \oplus ([c_j^j] \otimes [F_j^j]) \oplus$ 
      $\oplus (p_{j-1,j}^j \otimes (R_{j+1}^j [f_{j+1}^{j+1}])) \oplus [N_j^j]$ 
22:    $[u_j(t, [\Delta])] \leftarrow \hat{z}_j^\top [n_j^j]$ 
23: end for

```

previous desired trajectory at $t = t_p$. Then, one can satisfy the bounds described in Theorem 12 and Corollary 13 for all time.

This remark follows directly from the proofs of Theorem 12 and Corollary 13 by noticing that the arguments in their proofs hold for desired trajectories that are defined for all time rather than just for $t \in T$. One can then create a valid desired trajectory defined for all time by applying the strategy described in Rem. 14. This is the approach we adopt while performing receding horizon planning as described in Section VIII. To apply Rem. 14, one only needs to know the final state of the previous *desired trajectory* rather than the final state of the robot's *actual trajectory*.

B. Controller Implementation

The Interval Recursive Newton Euler Algorithm (IRNEA), introduced in [37], provides a means to efficiently compute the terms necessary to construct the nominal and robust inputs. IRNEA is described in Algorithm 1, where we have suppressed the dependence on $q_j(t)$ in R_j^{j-1} and p_j^{j-1} for convenience. The primary distinction between the classical Recursive Newton Euler Algorithm (RNEA) and IRNEA is that the latter takes in an interval set of inertial parameters and performs interval arithmetic operations in place of standard arithmetic operations. However, note that the first and third arguments to IRNEA are vectors and not intervals.

The nominal input τ can be directly computed using IRNEA:

$$\tau(q_A(t), \Delta_0) = \text{IRNEA}(q_A(t), \Delta_0, a_0^0) \quad (70)$$

where $a_0^0 = (0, 0, 9.81)^\top$ accounts for the effect of gravity. Note that by passing the nominal parameters Δ_0 (i.e., a degenerate interval) to IRNEA, the interval arithmetic computations in Algorithm 1 become standard arithmetic computations and IRNEA becomes identical to RNEA. Computing the robust input v is more involved, and requires computing bounds on the worst-case disturbance $w_M(q_A(t), \Delta_0, [\Delta])$ (63) and on the function given by $\underline{h}(q_A(t), [\Delta])$ (62).

The following lemma, whose proof can be found in Appendix C, describes how to use the IRNEA Algorithm to compute a w_M and a \underline{h} to satisfy the requirements of Theorem 12 and thereby compute the robust passivity-based controller.

Lemma 15 (Computing the Robust Input). *If the interval disturbance in (53) is computed as:*

$$[w(q_A(t), \Delta_0, [\Delta])] = \text{IRNEA}(q_A(t), [\Delta], a_0^0) - \tau(q_A(t), \Delta_0), \quad (71)$$

and we define w_M using the previous equation as:

$$w_M(q_A(t), \Delta_0, [\Delta]) := \rho([w(q_A(t), \Delta_0, [\Delta])]), \quad (72)$$

where ρ is as in Def. 9, then w_M satisfies (63) and is continuous in its first argument. Similarly, define $[V(q_A(t), [\Delta])]$ as

$$[V(q_A(t), [\Delta])] = \frac{1}{2} r(t)^\top [M(q(t), [\Delta]) r(t)]. \quad (73)$$

The term $[M(q(t), [\Delta]) r(t)]$ can be computed as

$$[M(q(t), [\Delta]) r(t)] = \text{IRNEA}(q_R(t), [\Delta], 0) \quad (74)$$

where $q_R(t)$ mirrors $q_A(t)$ (49)

$$q_R(t) = [q(t)^\top \quad 0^\top \quad q(t)^\top \quad 0^\top \quad r(t)^\top]^\top \quad (75)$$

and the base acceleration is set to 0 to exclude gravity in this computation. Because the velocity terms in $q_R(t)$ are set to zero, and gravity is excluded from the call to IRNEA, the output of $\text{IRNEA}(q_R(t), [\Delta], 0)$ excludes Coriolis and gravitational terms and directly yields $[M(q(t), [\Delta]) r(t)]$. If \underline{h} is defined as:

$$\underline{h}(q_A(t), [\Delta]) = -(\sup([V(q_A(t), [\Delta])])) + V_M, \quad (76)$$

then it satisfies (62) and is continuous in its first argument.

We note that the input computation in Lemma 15 runs quickly enough for real-time, safe operation, as we shown in Section X.

VIII. PLANNING ALGORITHM FORMULATION

The key technical idea of this work is to generate polynomial zonotope overapproximations of the trajectory and all constraints in the optimization problem (44)-(48) at the start of the planning iteration, then use these constraint overapproximations to perform optimization within t_p . Our approach guarantees safety while also ensuring:

- I. **Speed:** the size of all polynomial zonotope constraints can be fixed a priori, ensuring constraint evaluation is as fast as required.

- II. **Differentiability:** analytical gradients for use in optimization are generated via polynomial differentiation.
- III. **Continuous time and tracking error intervals:** each constraint is satisfied over the entire trajectory (including tracking error) for all time $t \in T$ rather than just at discretized time instances.
- IV. **Physical consistency:** dependencies between uncertain inertial parameters, such as the proportional coupling between a link's mass and its inertia matrix, can be modeled explicitly using polynomial zonotopes.

This section discusses the theory for representing these constraints using polynomial zonotopes and proves that these representations are overapproximative. This section concludes by describing how to transform the optimization problem (44)-(48) into an implementable version whose solutions can be followed by the robot in dynamically feasible and collision free fashion while satisfying input constraints. Sec. IX describes how to implement this framework.

A. Polynomial Zonotope Trajectory Representation

This subsection describes how ARMOUR overapproximates parameterized desired trajectories, as in Def. 8, to conservatively account for continuous time and tracking error within our optimization framework. Our approach to overapproximate trajectories of the robot applies polynomial zonotope arithmetic. Recall that as a result of Rem. 14, the initial condition of the desired trajectories at each planning iteration is known. As a result, the desired trajectories $q_d(t; k)$ are functions of only time t and the trajectory parameter k . Our approach begins by creating polynomial zonotope versions of T and K , which are then plugged into the formula for $q_d(t; k)$ to create polynomial zonotopes representing the desired trajectories.

1) *Time Horizon PZs:* To make this procedure rigorous, we first describe how to create polynomial zonotopes representing the time horizon T . Choose a timestep Δt so that $n_t := \frac{T}{\Delta t} \in \mathbb{N}$. Let $N_t := \{1, \dots, n_t\}$. Divide the compact time horizon $T \subset \mathbb{R}$ into n_t time subintervals. Consider the i^{th} time subinterval corresponding to $t \in [(i-1)\Delta t, i\Delta t]$. We represent this subinterval as a polynomial zonotope \mathbf{T}_i , where

$$\mathbf{T}_i = \left\{ t \in T \mid t = \frac{(i-1)+i}{2}\Delta t + \frac{1}{2}\Delta t x_{t_i}, x_{t_i} \in [-1, 1] \right\} \quad (77)$$

with indeterminate $x_{t_i} \in [-1, 1]$.

2) *Trajectory Parameter PZs:* Now we describe how to create polynomial zonotopes representing the set of trajectory parameters K . In this work, we choose $K = \bigtimes_{i=1}^{n_q} K_i$, where each K_j is a compact one-dimensional interval. For simplicity, we let each $K_j = [-1, 1]$. We represent the interval K_j as a polynomial zonotope $\mathbf{K}_j = x_{k_j}$ where $x_{k_j} \in [-1, 1]$ is an indeterminate. We let $x_k \in [-1, 1]^{n_q}$ denote the vector of indeterminates where the j^{th} component of x_k is x_{k_j} . With this choice of K_j , any particular k_j directly yields $k_j = \text{slice}(\mathbf{K}_j, x_{k_j}, k_j)$ (see (23)). In other words, plugging in k_j to the indeterminate x_{k_j} yields the subset of \mathbf{K}_j which is k_j itself. In fact, the process of “slicing” a polynomial zonotope by a trajectory parameter is critical to our formulation of the constraints within ARMOUR.

3) *Desired Trajectory PZs:* The desired position, velocity, and acceleration trajectories of the robot, defined in Def. 8, are functions of both time t and the trajectory parameter k . Using the time partition and trajectory parameter polynomial zonotopes described above, we create polynomial zonotopes $\mathbf{q}_{d,j}(\mathbf{T}_i; \mathbf{K})$ that overapproximate $q_{d,j}(t; k)$ for all t in the i^{th} time subinterval and $k \in K$ by plugging the polynomial zonotopes \mathbf{T}_i and \mathbf{K} into the formula for $q_{d,j}(t; k)$.

Lemma 16 (Desired Trajectory PZs). *The desired trajectory polynomial zonotopes $\mathbf{q}_{d,j}(\mathbf{T}_i; \mathbf{K})$ are overapproximative, i.e., for each $j \in N_q$, $\mathbf{q}_{d,j}(\mathbf{T}_i; \mathbf{K})$ satisfies*

$$q_{d,j}(t; k) \in \mathbf{q}_{d,j}(\mathbf{T}_i; \mathbf{K}) \quad \forall t \in \mathbf{T}_i, k \in \mathbf{K}. \quad (78)$$

One can similarly define $\dot{\mathbf{q}}_{d,j}(\mathbf{T}_i; \mathbf{K})$, and $\ddot{\mathbf{q}}_{d,j}(\mathbf{T}_i; \mathbf{K})$ that are also overapproximative.

Proof. The desired trajectory $q_{d,j}(t; k)$ is an analytic function that depends only on time t and k , which are included in \mathbf{T}_i and \mathbf{K} . All operations involving polynomial zonotopes are either exact or overapproximative for analytic functions [2, Section 2.D], so \mathbf{T}_i and \mathbf{K} in place of the arguments t and k yields an overapproximative polynomial zonotope. \square

4) *Slicing Yields Desired Trajectories:* Recall that \mathbf{T}_i and \mathbf{K}_j have indeterminates x_{t_i} and x_{k_j} respectively. Because the desired trajectories only depend on t and k , the polynomial zonotopes $\mathbf{q}_{d,j}(\mathbf{T}_i; \mathbf{K})$, $\dot{\mathbf{q}}_{d,j}(\mathbf{T}_i; \mathbf{K})$ and $\ddot{\mathbf{q}}_{d,j}(\mathbf{T}_i; \mathbf{K})$ depend only on the indeterminates x_{t_i} and x_k . By plugging in a given k for x_k via the `slice` operation, we obtain a polynomial zonotope where x_{t_i} is the only remaining indeterminate. Because we perform this particular slicing operation repeatedly throughout this document, if we are given a polynomial zonotope, $\mathbf{q}_{d,j}(\mathbf{T}_i; \mathbf{K})$, we use the shorthand $\mathbf{q}_{d,j}(\mathbf{T}_i; k) = \text{slice}(\mathbf{q}_{d,j}(\mathbf{T}_i; \mathbf{K}), x_k, k)$. Notice that because of our previous observation, $q_{d,j}(t; k) \in \mathbf{q}_{d,j}(\mathbf{T}_i; k)$ for all $t \in \mathbf{T}_i$ (and similarly for $\dot{\mathbf{q}}_{d,j}(\mathbf{T}_i; k)$ and $\ddot{\mathbf{q}}_{d,j}(\mathbf{T}_i; k)$).

5) *Incorporating Tracking Error:* Next, recall from Sec. VII that these desired trajectories can not be tracked perfectly by the robot. From Cor. 13, at each time t the position error of each joint $e_j(t)$ is bounded by $\varepsilon_{p,j}$, and the velocity error $\dot{e}_j(t)$ is bounded by ε_v . We use these to generate polynomial zonotopes that overapproximate any trajectory that is followed by the robot.

Lemma 17 (Error in Config. Space). *Let $\varepsilon_{p,j} = \varepsilon_{p,j} x_{e_{p,j}}$ and $\varepsilon_{v,j} = \varepsilon_{v,j} x_{e_{v,j}}$, with indeterminates $x_{e_{p,j}} \in [-1, 1]$ and $x_{e_{v,j}} \in [-1, 1]$. Then, let*

$$\mathbf{q}_j(\mathbf{T}_i; \mathbf{K}) = \mathbf{q}_{d,j}(\mathbf{T}_i; \mathbf{K}) \oplus \varepsilon_{p,j} \quad (79)$$

$$\dot{\mathbf{q}}_j(\mathbf{T}_i; \mathbf{K}) = \dot{\mathbf{q}}_{d,j}(\mathbf{T}_i; \mathbf{K}) \oplus \varepsilon_{v,j} \quad (80)$$

for each $i \in N_t$. Given the set of trajectory parameters \mathbf{K} , the polynomial zonotopes $\mathbf{q}_j(\mathbf{T}_i; \mathbf{K})$ and $\dot{\mathbf{q}}_j(\mathbf{T}_i; \mathbf{K})$ overapproximate the set of all joint trajectories that can possibly be executed by the robot, i.e., for each $j \in N_q$, $k \in \mathbf{K}$ we have

$$q_j(t; k) \in \mathbf{q}_j(\mathbf{T}_i; k) \quad \forall t \in \mathbf{T}_i \quad (81)$$

$$\dot{q}_j(t; k) \in \dot{\mathbf{q}}_j(\mathbf{T}_i; k) \quad \forall t \in \mathbf{T}_i \quad (82)$$

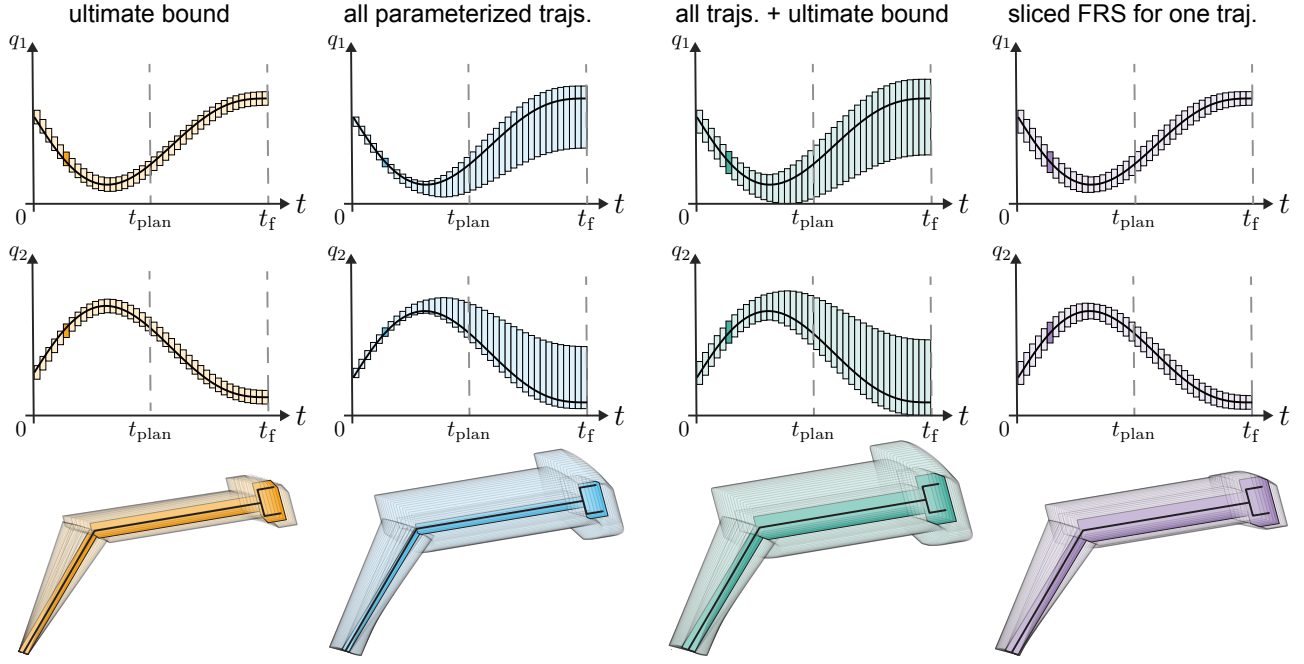


Fig. 2. Visualization of polynomial zonotope representations of the entire FRS and the subset corresponding to a single trajectory plan plus tracking error.

Proof. By Lem. 16, the desired trajectory polynomial zonotopes contain all desired trajectories. By Cor. 13, the position and velocity trajectories differ from the desired trajectories by at most $\pm \varepsilon_p$ and $\pm \varepsilon_v$, respectively. Therefore the Minkowski sum of $\mathbf{q}_{d,j}(\mathbf{T}_i; \mathbf{K}) \oplus \varepsilon_{p,j}$ must contain the actual configuration $q_j(t; k)$, and similarly for velocities. \square

Moving forward, let

$$\mathbf{q}_d(\mathbf{T}_i; \mathbf{K}) = \bigotimes_{j=1}^{n_q} \mathbf{q}_{d,j}(\mathbf{T}_i; \mathbf{K}), \quad (83)$$

$$\mathbf{q}(\mathbf{T}_i; \mathbf{K}) = \bigotimes_{j=1}^{n_q} \mathbf{q}_j(\mathbf{T}_i; \mathbf{K}). \quad (84)$$

We similarly define $\dot{\mathbf{q}}_d(\mathbf{T}_i; \mathbf{K})$, $\dot{\mathbf{q}}(\mathbf{T}_i; \mathbf{K})$, $\ddot{\mathbf{q}}_d(\mathbf{T}_i; \mathbf{K})$, and $\ddot{\mathbf{q}}(\mathbf{T}_i; \mathbf{K})$. Furthermore, let

$$\mathbf{E}_p = \bigotimes_{j=1}^{n_q} \varepsilon_{p,j}, \quad (85)$$

$$\mathbf{E}_v = \bigotimes_{j=1}^{n_q} \varepsilon_{v,j}. \quad (86)$$

B. Reachable Set Construction

After generating the polynomial zonotope overapproximations of joint trajectories in the previous subsection, ARMOUR composes these together to bound the kinematic behavior of the arm and the possible torques required to achieve these trajectories. We formulate algorithms which generate polynomial zonotopes (parameterized by k) describing the volume occupied by the arm and the motor torques required to track a given trajectory. These algorithms run at the beginning of each planning iteration, and their outputs are used to formulate constraints on k which overapproximate those in (45) - (48). In

the remainder of this subsection, we describe how to compute reachable sets for a single joint/link over a single interval of time.

1) *Forward Kinematics Reachable Set:* We reformulate the robot's forward kinematics (36) using polynomial zonotope overapproximations of the joint position trajectories (79). Using $\mathbf{q}_j(\mathbf{T}_i; \mathbf{K})$ we can compute $\mathbf{p}_j^{j-1}(\mathbf{q}_j(\mathbf{T}_i; \mathbf{K}))$ and $\mathbf{R}_j^{j-1}(\mathbf{q}_j(\mathbf{T}_i; \mathbf{K}))$, which represent overapproximations of the position and orientation of the j^{th} frame with respect to frame $(j-1)$ at the i^{th} time step.

The rotation matrix $R_j^{j-1}(q_j(t; k))$ depends on $\cos(q_j(t; k))$ and $\sin(q_j(t; k))$. Because we represent a set of the j^{th} joint's angles for the i^{th} time step using the polynomial zonotope $\mathbf{q}_j(\mathbf{T}_i; \mathbf{K})$, we must compute $\cos(\mathbf{q}_j(\mathbf{T}_i; \mathbf{K}))$ and $\sin(\mathbf{q}_j(\mathbf{T}_i; \mathbf{K}))$ to compute $\mathbf{R}_j^{j-1}(\mathbf{q}_j(\mathbf{T}_i; \mathbf{K}))$. Cosine and sine are analytic functions, and so we can compute $\cos(\mathbf{q}_j(\mathbf{T}_i; \mathbf{K}))$ and $\sin(\mathbf{q}_j(\mathbf{T}_i; \mathbf{K}))$ using Taylor expansions as in (31). In practice, only a finite degree Taylor expansion can be constructed and the Lagrange Remainder as described in Sec. III-D is used to conservatively bound the truncation error. By using this property and the fact that all operations involving polynomial zonotopes are either exact or overapproximative, the polynomial zonotope forward kinematics can be computed similarly to the classical formulation (36) and proven to be overapproximative:

Lemma 18 (PZ Forward Kinematics). *Let the polynomial zonotope forward kinematics for the j^{th} frame at the i^{th} time step be defined as*

$$\mathbf{FK}_j(\mathbf{q}(\mathbf{T}_i; \mathbf{K})) = \begin{bmatrix} \mathbf{R}_j(\mathbf{q}(\mathbf{T}_i; \mathbf{K})) & \mathbf{p}_j(\mathbf{q}(\mathbf{T}_i; \mathbf{K})) \\ \mathbf{0} & 1 \end{bmatrix}, \quad (87)$$

Algorithm 2: $\{\mathbf{FK}_j(\mathbf{q}(\mathbf{T}_i; \mathbf{K})) : j \in N_q\} = \text{PZFK}(\mathbf{q}(\mathbf{T}_i; \mathbf{K}))$

```

1:  $\mathbf{p}_0(\mathbf{q}(\mathbf{T}_i; \mathbf{K})) \leftarrow 0$ 
2:  $\mathbf{R}_0(\mathbf{q}(\mathbf{T}_i; \mathbf{K})) \leftarrow \mathbf{I}_{3 \times 3}$ 
3: for  $j = 1 : n_q$ 
4:    $\mathbf{R}_j^{j-1}(\mathbf{q}_j(\mathbf{T}_i; \mathbf{K})), \mathbf{p}_j^{j-1} \leftarrow \mathbf{H}_j^{j-1}(\mathbf{q}_j(\mathbf{T}_i; \mathbf{K}))$  as in (35)
5:    $\mathbf{p}_j(\mathbf{q}(\mathbf{T}_i; \mathbf{K})) \leftarrow \mathbf{p}_{j-1}(\mathbf{q}(\mathbf{T}_i; \mathbf{K})) \oplus \mathbf{R}_{j-1}(\mathbf{q}(\mathbf{T}_i; \mathbf{K})) \mathbf{p}_j^{j-1}$ 
6:    $\mathbf{R}_j(\mathbf{q}(\mathbf{T}_i; \mathbf{K})) \leftarrow \mathbf{R}_{j-1}(\mathbf{q}(\mathbf{T}_i; \mathbf{K})) \mathbf{R}_j^{j-1}(\mathbf{q}_j(\mathbf{T}_i; \mathbf{K}))$ 
7:    $\mathbf{FK}_j(\mathbf{q}(\mathbf{T}_i; \mathbf{K})) \leftarrow \{\mathbf{R}_j(\mathbf{q}(\mathbf{T}_i; \mathbf{K})), \mathbf{p}_j(\mathbf{q}(\mathbf{T}_i; \mathbf{K}))\}$ 
8: end for

```

where

$$\mathbf{R}_j(\mathbf{q}(\mathbf{T}_i; \mathbf{K})) = \prod_{l=1}^j \mathbf{R}_l^{l-1}(\mathbf{q}_l(\mathbf{T}_i; \mathbf{K})) \quad (88)$$

and

$$\mathbf{p}_j(\mathbf{q}(\mathbf{T}_i; \mathbf{K})) = \sum_{l=1}^j \mathbf{R}_l(\mathbf{q}(\mathbf{T}_i; \mathbf{K})) \mathbf{p}_l^{l-1}, \quad (89)$$

then for each $j \in N_q$, $k \in \mathbf{K}$, $\mathbf{FK}_j(\mathbf{q}(t; k)) \in \mathbf{FK}_j(\mathbf{q}(\mathbf{T}_i; k))$ for all $t \in \mathbf{T}_i$.

The Polynomial Zonotope Forward Kinematics Algorithm (PZFK), detailed in Alg. 2, is used to compute the objects in Lem. 18 from the set of possible configurations $\mathbf{q}(\mathbf{T}_i; \mathbf{K})$.

2) *Forward Occupancy Reachable Set:* To guarantee safety, it is necessary to ensure that the robot never collides with any obstacles for all time. To accomplish this, we overapproximate the forward occupancy (39) of each link over every time interval. By applying the forward kinematics reachable set (87) and the fact that all operations involving polynomial zonotopes are either exact or overapproximative, the polynomial zonotope forward occupancy reachable set can be computed and proven to be overapproximative:

Lemma 19 (PZ Forward Occupancy). *Let the j^{th} link of the robot be overapproximated by a polynomial zonotope denoted by \mathbf{L}_j and the polynomial zonotope forward occupancy reachable set for the j^{th} link at the i^{th} time step be defined as:*

$$\mathbf{FO}_j(\mathbf{q}(\mathbf{T}_i; \mathbf{K})) = \mathbf{p}_j(\mathbf{q}(\mathbf{T}_i; \mathbf{K})) \oplus \mathbf{R}_j(\mathbf{q}(\mathbf{T}_i; \mathbf{K})) \mathbf{L}_j, \quad (90)$$

then for each $j \in N_q$, $k \in \mathbf{K}$, $\mathbf{FO}_j(\mathbf{q}(t; k)) \in \mathbf{FO}_j(\mathbf{q}(\mathbf{T}_i; k))$ for all $t \in \mathbf{T}_i$.

In Sec. VIII-C, we describe how the forward occupancy reachable set is used to compute collision-avoidance constraints. For convenience, let

$$\mathbf{FO}(\mathbf{q}(\mathbf{T}_i; \mathbf{K})) = \bigcup_{j=1}^{n_q} \mathbf{FO}_j(\mathbf{q}(\mathbf{T}_i; \mathbf{K})). \quad (91)$$

3) *Input Reachable Set:* In addition to constraining the pose of the robot and avoiding collisions, mobile manipulators must avoid saturating their available motor torques. We next describe how to overapproximate the set of torques that may be required for the robust passivity-based control input (51) to track any parameterized trajectory. Just as we did in Sec. VII (49), we begin by defining a total feedback trajectory polynomial zonotope $\mathbf{q}_A(\mathbf{T}_i; \mathbf{K})$ by computing a polynomial zonotope representation of each of the components of \mathbf{q}_A .

Algorithm 3:
 $\{\mathbf{u}_j(\mathbf{q}_A(\mathbf{T}_i; \mathbf{K}), [\Delta]) : j \in N_q\} = \text{PZRNEA}(\mathbf{q}_A(\mathbf{T}_i; \mathbf{K}), [\Delta], a_0^0)$

```

1: Compute  $\dot{\mathbf{q}}_a(\mathbf{T}_i; \mathbf{K})$  and  $\ddot{\mathbf{q}}_a(\mathbf{T}_i; \mathbf{K})$  using (92)
2: Initialize base acceleration  $a_0^0$ .
3: for  $j = 1 : n_q$ 
4:    $\mathbf{R}_j^{j-1}, \mathbf{p}_j^{j-1} \leftarrow \mathbf{H}_j^{j-1}(\mathbf{q}_j(\mathbf{T}_i; \mathbf{K}))$ 
5:    $\mathbf{R}_{j-1}^j \leftarrow \text{pzTranspose}(\mathbf{R}_j^{j-1})$ 
6: end for
7: for  $j = 1 : n_q$ 
8:    $\omega_j^j \leftarrow \mathbf{R}_{j-1}^j \omega_{j-1}^{j-1} \oplus \dot{\mathbf{q}}_j(t) \hat{z}_j$ 
9:    $\omega_{a,j}^j \leftarrow \mathbf{R}_{j-1}^j \omega_{a,j-1}^{j-1} \oplus \ddot{\mathbf{q}}_{a,j}(t) \hat{z}_j$ 
10:   $\dot{\omega}_j^j \leftarrow \mathbf{R}_{j-1}^j \dot{\omega}_{j-1}^{j-1} \oplus ((\mathbf{R}_{j-1}^j \omega_{a,j-1}^{j-1}) \otimes (\dot{\mathbf{q}}_j(t) \hat{z}_j)) \oplus \ddot{\mathbf{q}}_{a,j} \hat{z}_j$ 
11:   $\mathbf{a}_j^j \leftarrow (\mathbf{R}_{j-1}^j \mathbf{a}_{j-1}^{j-1}) \oplus (\dot{\omega}_j^j \otimes \mathbf{p}_j^{j-1}) \oplus (\omega_j^j \otimes (\omega_{a,j}^j \times \mathbf{p}_j^{j-1}))$ 
12:   $\mathbf{a}_{c,j}^j \leftarrow \mathbf{a}_j^j \oplus (\dot{\omega}_j^j \otimes \mathbf{c}_j^j) \oplus (\omega_j^j \otimes (\omega_{a,j}^j \otimes \mathbf{c}_j^j))$ 
13:   $\mathbf{F}_j^j \leftarrow \mathbf{m}_j \mathbf{a}_{c,j}^j$ 
14:   $\mathbf{N}_j^j \leftarrow \mathbf{I}_j^j \dot{\omega}_j^j \oplus (\omega_{a,j}^j \otimes (\mathbf{I}_j^j \omega_j^j))$ 
15: end for
16:  $\mathbf{R}_{n_q+1}^{n_q} \leftarrow \mathbf{I}_{3 \times 3}$ 
17:  $\mathbf{f}_{n_q+1}^{n_q+1} \leftarrow 0$ 
18:  $\mathbf{n}_{n_q+1}^{n_q+1} \leftarrow 0$ 
19: for  $j = n_q : -1 : 1$ 
20:    $\mathbf{f}_j^j \leftarrow (\mathbf{R}_{j+1}^j \mathbf{f}_{j+1}^{j+1}) \oplus \mathbf{F}_j^j$ 
21:    $\mathbf{n}_j^j \leftarrow (\mathbf{R}_{j+1}^j \mathbf{n}_{j+1}^{j+1}) \oplus (\mathbf{c}_j^j \otimes \mathbf{F}_j^j) \oplus$ 
      $\oplus (\mathbf{p}_{j-1}^j \otimes (\mathbf{R}_{j+1}^j \mathbf{f}_{j+1}^{j+1})) \oplus \mathbf{N}_j^j$ 
22:    $\mathbf{u}_j(\mathbf{q}_A(\mathbf{T}_i; \mathbf{K}), [\Delta]) \leftarrow \hat{z}_j^\top \mathbf{n}_j^j$ 
23: end for

```

We also define modified desired velocity and acceleration trajectory polynomial zonotopes that are composed of desired trajectories plus a gain matrix times tracking error:

$$\begin{aligned} \dot{\mathbf{q}}_a(\mathbf{T}_i; \mathbf{K}) &= \mathbf{q}_d(\mathbf{T}_i; \mathbf{K}) \oplus K_r \mathbf{E}_p, \\ \ddot{\mathbf{q}}_a(\mathbf{T}_i; \mathbf{K}) &= \dot{\mathbf{q}}_d(\mathbf{T}_i; \mathbf{K}) \oplus K_r \mathbf{E}_v. \end{aligned} \quad (92)$$

Using these definitions and plugging into (52), we obtain

$$\begin{aligned} \boldsymbol{\tau}(\mathbf{q}_A(\mathbf{T}_i; \mathbf{K}), \Delta_0) &= \mathbf{M}(\mathbf{q}(\mathbf{T}_i; \mathbf{K}), \Delta_0) \ddot{\mathbf{q}}_a(\mathbf{T}_i; \mathbf{K}) + \\ &+ \mathbf{C}(\mathbf{q}(\mathbf{T}_i; \mathbf{K}), \dot{\mathbf{q}}(\mathbf{T}_i; \mathbf{K}), \Delta_0) \dot{\mathbf{q}}_a(\mathbf{T}_i; \mathbf{K}) + \\ &+ \mathbf{G}(\mathbf{q}(\mathbf{T}_i; \mathbf{K}), \Delta_0). \end{aligned} \quad (93)$$

As written in (93), the computation of the nominal input $\boldsymbol{\tau}(\mathbf{q}_A(\mathbf{T}_i; \mathbf{K}), \Delta_0)$ requires finding the mass matrix and Coriolis and gravitational terms. Instead, a more direct approach is to use a modified Recursive Newton-Euler Algorithm (RNEA) to compute $\boldsymbol{\tau}(\mathbf{q}_A(\mathbf{T}_i; \mathbf{K}), \Delta_0)$, which circumvents the computation of these terms. Here, we introduce the Polynomial Zonotope RNEA (PZRNEA), detailed in Alg. 3. Note just as in the original RNEA and IRNEA Algorithms, we have suppressed the dependence on $\mathbf{q}_j(\mathbf{T}_i; \mathbf{K})$ in \mathbf{R}_{j-1}^j . PZRNEA takes as inputs $\mathbf{q}_A(\mathbf{T}_i; \mathbf{K})$, and the nominal inertial parameters Δ_0 to find the nominal input:

$$\boldsymbol{\tau}(\mathbf{q}_A(\mathbf{T}_i; \mathbf{K}), \Delta_0) = \text{PZRNEA}(\mathbf{q}_A(\mathbf{T}_i; \mathbf{K}), \Delta_0, a_0^0), \quad (94)$$

where $a_0^0 = (0, 0, 9.81)^\top$.

Next, we describe a bound on the robust control input (65) at each time step whose proof can be found in Appendix E.

Theorem 20 (Robust Input Bound). Suppose $\alpha : \mathbb{R} \rightarrow \mathbb{R}$ in (66) is a linear function, i.e.,

$$\alpha(x) = \alpha_c x \quad (95)$$

where $\alpha_c > 0$ is a user-specified constant. Suppose as in (71), the disturbance (53) is overapproximated using

$$\mathbf{w}(\mathbf{q}_A(\mathbf{T}_i; \mathbf{K}), \Delta_0, [\Delta]) = \text{PZRNEA}(\mathbf{q}_A(\mathbf{T}_i; \mathbf{K}), [\Delta], a_0^0) + \boldsymbol{\tau}(\mathbf{q}_A(\mathbf{T}_i; \mathbf{K}), \Delta_0) \quad (96)$$

with PZRNEA as in Alg. 3 and $a_0^0 = [0, 0, 9.81]^\top$. Using Def. 9, let

$$\rho(\mathbf{w}(\mathbf{q}_A(\mathbf{T}_i; \mathbf{K}), \Delta_0, [\Delta])) = \max \left(\left| \inf(\mathbf{w}(\mathbf{q}_A(\mathbf{T}_i; \mathbf{K}), \Delta_0, [\Delta])) \right|, \left| \sup(\mathbf{w}(\mathbf{q}_A(\mathbf{T}_i; \mathbf{K}), \Delta_0, [\Delta])) \right| \right), \quad (97)$$

and as in (72) let

$$w_M(\star) = \rho(\mathbf{w}(\mathbf{q}_A(\mathbf{T}_i; \mathbf{K}), \Delta_0, [\Delta])) \quad (98)$$

where $w_M(\star) := w_M(\mathbf{q}_A(\mathbf{T}_i; \mathbf{K}), \Delta_0, [\Delta])$. Then for all $q_A(t; k)$ that satisfies the uniform bound (67), the following bound is satisfied for each $j \in N_q$

$$\left| v(q_A(t; k), \Delta_0, [\Delta])_j \right| \leq \frac{\alpha_c \mathcal{E}(\sigma_M - \sigma_m)}{2} + \frac{\|w_M(\star)\| + w_M(\star)_j}{2}, \quad (99)$$

where $|v(q_A(t; k), \Delta_0, [\Delta])_j|$ is the j^{th} component of the robust input.

Note that this theorem describes a bound on the robust input term in (51); however, it requires that α in the definition of (66) is a linear function with positive slope rather than an arbitrary extended class \mathcal{K}_∞ function. The proof could be extended to any extended class \mathcal{K}_∞ function, but would generate a bound that would be more difficult to compute in real-time. Nevertheless, as we show in Sec. X, this type of linear α works well in practice. Using (99), we bound the robust input by a constant in each dimension. That is, we let

$$\mathbf{v}_j(\mathbf{q}_A(\mathbf{T}_i; \mathbf{K}), \Delta_0, [\Delta]) = \left(\frac{\alpha_c \mathcal{E}(\sigma_M - \sigma_m)}{2} + \frac{\|w_M(\star)\| + w_M(\star)_j}{2} \right) x_{v_j} \quad (100)$$

with $w_M(\star)$ as in Thm. 20 and x_{v_j} an indeterminate in $[-1, 1]$. Using this we let

$$\mathbf{v}(\mathbf{q}_A(\mathbf{T}_i; \mathbf{K}), \Delta_0, [\Delta]) = \bigotimes_{j=1}^{n_q} \mathbf{v}_j(\mathbf{q}_A(\mathbf{T}_i; \mathbf{K}), \Delta_0, [\Delta]). \quad (101)$$

Finally, we define the *input reachable set* for the i^{th} timestep as

$$\mathbf{u}(\mathbf{q}_A(\mathbf{T}_i; \mathbf{K}), \Delta_0, [\Delta]) = \boldsymbol{\tau}(\mathbf{q}_A(\mathbf{T}_i; \mathbf{K}), \Delta_0) + \mathbf{v}(\mathbf{q}_A(\mathbf{T}_i; \mathbf{K}), \Delta_0, [\Delta]). \quad (102)$$

Note that because the robust input bound is treated as constant in each dimension (100), when we slice the input reachable

set by k , we only slice the polynomial zonotope representation of the nominal input by k , i.e.,

$$\mathbf{u}(\mathbf{q}_A(\mathbf{T}_i; k), \Delta_0, [\Delta]) = \boldsymbol{\tau}(\mathbf{q}_A(\mathbf{T}_i; k), \Delta_0) + \mathbf{v}(\mathbf{q}_A(\mathbf{T}_i; \mathbf{K}), \Delta_0, [\Delta]). \quad (103)$$

Using these definitions, we prove that the input reachable set contains the robust passivity-based control input (51):

Lemma 21 (Input PZ Conservativeness). The input reachable set is overapproximative, i.e., for each $k \in \mathbf{K}$

$$\mathbf{u}(q_A(t; k), \Delta_0, [\Delta]) \in \mathbf{u}(\mathbf{q}_A(\mathbf{T}_i; k), \Delta_0, [\Delta]) \quad \forall t \in \mathbf{T}_i. \quad (104)$$

Proof. The polynomial zonotope bound of the nominal input $\boldsymbol{\tau}(\mathbf{q}_A(\mathbf{T}_i; k), \Delta_0)$ is constructed using Alg. 3. Because all operations in Alg. 3 involve polynomial zonotopes with an input that is an overapproximation to $q_A(t; k)$, the output of the algorithm is an overapproximation to $\boldsymbol{\tau}(q_A(t; k), \Delta_0)$. The result then follows by applying Theorem 20 and (102). \square

C. Constraint Generation

We now have all the necessary components to pose the trajectory optimization constraints using polynomial zonotopes.

1) *Joint Limit Constraints:* The polynomial zonotopes $\mathbf{q}_j(\mathbf{T}_i; \mathbf{K})$ and $\dot{\mathbf{q}}_j(\mathbf{T}_i; \mathbf{K})$ from (79) and (80) incorporate tracking error and overapproximate all reachable joint angles and velocities over each time step. Therefore, choosing k such that $\mathbf{q}_j(\mathbf{T}_i; k)$ and $\dot{\mathbf{q}}_j(\mathbf{T}_i; k)$ are completely contained within $[q_{j,\text{lim}}^-, q_{j,\text{lim}}^+]$ and $[\dot{q}_{j,\text{lim}}^-, \dot{q}_{j,\text{lim}}^+]$ respectively ensures that joint position and velocity limits are always satisfied.

2) *Collision Avoidance Constraints:* The forward occupancy of each of the robot's links is overapproximated by $\mathbf{FO}_j(\mathbf{q}(\mathbf{T}_i; \mathbf{K}))$ given in (90). The robot must never collide with obstacles, which is guaranteed by choosing k such that $\mathbf{FO}_j(\mathbf{q}(\mathbf{T}_i; k)) \cap \mathcal{O} = \emptyset$.

3) *Input Constraints:* The input polynomial zonotope $\mathbf{u}(\mathbf{q}_A(\mathbf{T}_i; \mathbf{K}), \Delta_0, [\Delta])$ is formed by applying (102). Importantly, the disturbances (caused by inertial parameter mismatch) and tracking error are not known at the time of planning. The input polynomial zonotopes deal with these conservatively by assuming the worst-case disturbances and tracking error possible. Choosing k such that $\mathbf{u}(\mathbf{q}_A(\mathbf{T}_i; k), \Delta_0, [\Delta]) \subseteq [u_{j,\text{lim}}^-, u_{j,\text{lim}}^+]$ ensures that torque limits are not violated when tracking a desired trajectory.

D. Trajectory Optimization

To conclude this section, we combine these polynomial zonotope constraints within a trajectory optimization program. We seek to minimize a user-specified cost (such as reaching a desired intermediate waypoint) while strictly satisfying each safety constraint.

$$\min_{k \in \mathbf{K}} \text{cost}(k) \quad (105)$$

$$\mathbf{q}_j(\mathbf{T}_i; k) \subseteq [q_{j,\text{lim}}^-, q_{j,\text{lim}}^+] \quad \forall i \in N_t, j \in N_q \quad (106)$$

$$\dot{\mathbf{q}}_j(\mathbf{T}_i; k) \subseteq [\dot{q}_{j,\text{lim}}^-, \dot{q}_{j,\text{lim}}^+] \quad \forall i \in N_t, j \in N_q \quad (107)$$

$$\mathbf{u}(\mathbf{q}_A(\mathbf{T}_i; k), \Delta_0, [\Delta]) \subseteq [u_{j,\text{lim}}^-, u_{j,\text{lim}}^+] \quad \forall i \in N_t, j \in N_q \quad (108)$$

$$\mathbf{FO}_j(\mathbf{q}(\mathbf{T}_i; k)) \cap \mathcal{O} = \emptyset \quad \forall i \in N_t, j \in N_q. \quad (109)$$

Finally, by applying Lemmas 17, 18, and 21 one can prove that any feasible solution to this optimization problem can be tracked safely by the robot:

Lemma 22 (Traj. Opt. Safety). *Suppose $k \in K$ is a feasible solution to (105), then k can be tracked for all t in T by the robot while satisfying joint limits, input limits, and without colliding into any obstacles.*

IX. ARMOUR IMPLEMENTATION

This section describes our implementation of the planning algorithm formulated in Section VIII and how to apply it while performing real-time control in dynamically feasible fashion while avoiding obstacles and satisfying input constraints. To simplify exposition in Section IX-A, we begin by proposing an example desired trajectory that satisfies Definition 8 and describe how to construct a polynomial zonotope overapproximation to it as was described in Section VIII-A. Next in Section IX-B, we describe how to use this polynomial zonotope representation to write down constraints (106)-(109). Finally in Section IX-C, we summarize the online operation of ARMOUR.

A. An Example Desired Trajectory

This work uses degree 5 Bernstein polynomials to parameterize the desired trajectories of the arm. Letting $T = [0, 1]$, the Bernstein polynomials take the form

$$q_{d,j}(t; k) = \sum_{l=0}^5 \beta_{j,l}(k) b_{j,l}(t), \quad (110)$$

where $\beta_{j,l}(k) \in \mathbb{R}$ are the Bernstein Coefficients and $b_{j,l} : T \rightarrow \mathbb{R}$ are the Bernstein Basis Polynomials of degree 5 given by

$$b_{j,l}(t) = \binom{5}{l} t^l (1-t)^{5-l}, \quad (111)$$

for each $l \in \{0, \dots, 5\}$. Notice from Definition 8 that the first and second properties of trajectory parameters constrain the initial position, velocity, and acceleration of the trajectory to match the initial condition, and require the final velocity and acceleration to be 0. These properties fix five of the six Bernstein coefficients $\beta_{j,v}$ as

$$\beta_{j,0}(k) = q_{d,j_0} \quad (112)$$

$$\beta_{j,1}(k) = \frac{1}{5}(\dot{q}_{d,j_0} + 5\beta_{j,0}) \quad (113)$$

$$\beta_{j,2}(k) = \frac{1}{20}(\ddot{q}_{d,j_0} + 40\beta_{j,1} - 20\beta_{j,0}) \quad (114)$$

$$\beta_{j,3}(k) = \frac{1}{20}(0 + 40\beta_{j,4} - 20\beta_{j,5}) \quad (115)$$

$$\beta_{j,4}(k) = \frac{1}{5}(0 + 5\beta_{j,5}). \quad (116)$$

Note because the first five Bernstein coefficients are fixed, they are not a function of the trajectory parameter, so we drop the dependence on k for these coefficients. We let the last coefficient $\beta_{j,5}$ be

$$\beta_{j,5}(k) = \eta_{j,1}k_j + \eta_{j,2} \quad (117)$$

where $\eta_{j,1}$ and $\eta_{j,2} \in \mathbb{R}$ are user-specified constants. The coefficient $\beta_{j,5}$ equals the final position $q_j(1; k)$ at time $t = 1$, so the choice of trajectory parameter k_j determines this value.

We construct the polynomial zonotope representation $\mathbf{q}_{d,j}(\mathbf{T}_i; \mathbf{K})$ by plugging in \mathbf{T}_i from (77) and \mathbf{K}_j . Letting $\beta_{j,5}(\mathbf{K}) = \eta_{j,1}\mathbf{K}_j + \eta_{j,2}$, and plugging \mathbf{T}_i into the basis polynomials (111), we obtain

$$\mathbf{q}_{d,j}(\mathbf{T}_i; \mathbf{K}) = \left(\sum_{l=0}^4 \beta_{j,l} \mathbf{b}_{j,l}(\mathbf{T}_i) \right) \oplus \beta_{j,5}(\mathbf{K}) \mathbf{b}_{j,5}(\mathbf{T}_i), \quad (118)$$

The desired velocity and acceleration polynomial zonotopes $\dot{\mathbf{q}}_{d,j}(\mathbf{T}_i; \mathbf{K})$ and $\ddot{\mathbf{q}}_{d,j}(\mathbf{T}_i; \mathbf{K})$ can be similarly computed. These desired trajectory polynomial zonotopes are combined with the tracking error polynomial zonotopes to get $\mathbf{q}(\mathbf{T}_i; \mathbf{K})$ and $\dot{\mathbf{q}}(\mathbf{T}_i; \mathbf{K})$ as in (79) and (80), as well as $\dot{\mathbf{q}}_a(\mathbf{T}_i; \mathbf{K})$ and $\ddot{\mathbf{q}}_a(\mathbf{T}_i; \mathbf{K})$ as in (92). To summarize, by specifying the initial condition of the desired trajectory, *i.e.*, $(q_{d0}, \dot{q}_{d0}, \ddot{q}_{d0})$, one can construct the polynomial zonotope representation of the desired trajectory and all of its variants.

B. Constraints

We now implement joint limits, collision avoidance, and input constraints. Recall that \sup and \inf overapproximate the bounds of a polynomial zonotope explicitly as in (24) and (25), meaning that we do not need to optimize over the elements of a PZ to compute any of the following constraints.

1) *Joint Limit Constraints*: We generate constraints that ensure that the subsets of possible joint positions $\mathbf{q}(\mathbf{T}_i; k)$ and joint velocities $\dot{\mathbf{q}}(\mathbf{T}_i; k)$ for a given $k \in \mathbf{K}$ are within the allowable joint limits. We let

$$h_{q-}(i, j, k) = -(\inf(\mathbf{q}_j(\mathbf{T}_i; k)) - q_{j,\lim}^-) \quad (119)$$

$$h_{q+}(i, j, k) = -(q_{j,\lim}^+ - \sup(\mathbf{q}_j(\mathbf{T}_i; k))) \quad (120)$$

where $h_{q-}(i, j, k) \leq 0$ and $h_{q+}(i, j, k) \leq 0$ ensure that the joint position limits are satisfied. Similarly, let

$$h_{\dot{q}-}(i, j, k) = -(\inf(\dot{\mathbf{q}}_j(\mathbf{T}_i; k)) - \dot{q}_{j,\lim}^-) \quad (121)$$

$$h_{\dot{q}+}(i, j, k) = -(\dot{q}_{j,\lim}^+ - \sup(\dot{\mathbf{q}}_j(\mathbf{T}_i; k))) \quad (122)$$

where $h_{\dot{q}-}(i, j, k) \leq 0$ and $h_{\dot{q}+}(i, j, k) \leq 0$ ensure the joint velocity limits are satisfied.

2) *Collision Avoidance Constraints*: The forward occupancy PZ $\mathbf{FO}_j(\mathbf{q}(\mathbf{T}_i; \mathbf{K}))$ produced by (90) overapproximates all reachable positions of points on the j^{th} link for the i^{th} time subinterval. Our goal is to generate constraints which ensure that the subset of $\mathbf{FO}_j(\mathbf{q}(\mathbf{T}_i; \mathbf{K}))$ for a particular k do not intersect with any obstacles $O \in \mathcal{O}$. These constraints are similar to those in [3, Section 4], but are updated to use the more general polynomial zonotope set representation.

Because the obstacles are convex polytopes (Assum. 5), one can compute a halfspace representation of obstacle O given by $A_O \in \mathbb{R}^{n_f \times 3}$ and $b_O \in \mathbb{R}^{n_f}$, where n_f is the number of faces of O . A point $p_1 \in \mathbb{R}^3$ is contained within the obstacle if and only if $A_O p_1 - b_O \leq 0$, where the inequality is taken element-wise. Therefore, p_1 lies outside the obstacle if any of the inequalities do not hold. More succinctly, $p_1 \notin O \iff \max(A_O p_1 - b_O) > 0$, where the max is taken element-wise. This implies that $\mathbf{FO}_j(\mathbf{q}(\mathbf{T}_i; k)) \cap O = \emptyset \iff \max(A_O p_1 - b_O) > 0, \forall p_1 \in \mathbf{FO}_j(\mathbf{q}(\mathbf{T}_i; k))$. The expression $A_O \mathbf{FO}_j(\mathbf{q}(\mathbf{T}_i; k)) - b_O$ yields an $n_f \times 1$ polynomial zonotope.

The constraint that $\mathbf{FO}_j(\mathbf{q}(\mathbf{T}_i; k))$ does not intersect O can be written as $h_{\text{obs}}(i, j, k, O) < 0$, where

$$h_{\text{obs}}(i, j, k, O) = -\max(\inf(A_O \mathbf{FO}_j(\mathbf{q}(\mathbf{T}_i; k)) - b_O)) \quad (123)$$

and the max is taken element-wise.

3) *Input Constraints*: The nominal input polynomial zonotope $\boldsymbol{\tau}(\mathbf{q}_A(\mathbf{T}_i; \mathbf{K}), \Delta_0)$ is computed using PZRNEA as in (94). As discussed in Lemma 20, we use PZRNEA to assist in constructing the robust input bound that generates $\mathbf{v}(\mathbf{q}_A(\mathbf{T}_i; \mathbf{K}), \Delta_0, [\Delta])$ (101) as well. First, we construct $\mathbf{w}(\mathbf{q}_A(\mathbf{T}_i; \mathbf{K}), \Delta_0, [\Delta])$ using PZRNEA as in (96). Plugging $\mathbf{w}(\mathbf{q}_A(\mathbf{T}_i; \mathbf{K}), \Delta_0, [\Delta])$, the uniform bound (64), the eigenvalue bounds from Assumption 11, and the form of α as in (95) into (100), we may construct $\mathbf{v}(\mathbf{q}_A(\mathbf{T}_i; \mathbf{K}), \Delta_0, [\Delta])$ as in (101). Finally, combining $\boldsymbol{\tau}(\mathbf{q}_A(\mathbf{T}_i; \mathbf{K}), \Delta_0)$ and $\mathbf{v}(\mathbf{q}_A(\mathbf{T}_i; \mathbf{K}), \Delta_0, [\Delta])$ yields $\mathbf{u}(\mathbf{q}_A(\mathbf{T}_i; k), \Delta_0, [\Delta])$ as in (102), which is then used to construct input constraints for a polynomial optimization problem. In particular, we let

$$h_{u^-}(i, j, k) = -(\inf(\mathbf{u}_j(\mathbf{T}_i; k)) - u_{j, \text{lim}}^-) \quad (124)$$

$$h_{u^+}(i, j, k) = -(u_{j, \text{lim}}^+ - \sup(\mathbf{u}_j(\mathbf{T}_i; k))) \quad (125)$$

where $h_{u^-}(i, j, k) < 0$ and $h_{u^+}(i, j, k) < 0$ ensures the input limits are satisfied.

C. Trajectory Optimization

Taking each of these constraints together, we can present an implementable version of the optimization program found in Section VIII-D:

$$\min_{k \in K} \text{cost}(k) \quad (126)$$

$$h_{q^-}(i, j, k) \leq 0, \quad \forall i \in N_t, j \in N_q \quad (127)$$

$$h_{q^+}(i, j, k) \leq 0 \quad \forall i \in N_t, j \in N_q \quad (128)$$

$$h_{\dot{q}^-}(i, j, k) \leq 0 \quad \forall i \in N_t, j \in N_q \quad (129)$$

$$h_{\dot{q}^+}(i, j, k) \leq 0 \quad \forall i \in N_t, j \in N_q \quad (130)$$

$$h_{u^-}(i, j, k) \leq 0 \quad \forall i \in N_t, j \in N_q \quad (131)$$

$$h_{u^+}(i, j, k) \leq 0 \quad \forall i \in N_t, j \in N_q \quad (132)$$

$$h_{\text{obs}}(i, j, k, O) < 0 \quad \forall i \in N_t, j \in N_q, O \in \mathcal{O}. \quad (133)$$

The solver and hyperparameters used to solve this nonlinear program are detailed in Section X-A7. Note that each of these constraints can be represented for each time interval i in N_t in parallel. By applying Lemma 22 one can prove that any feasible solution to this optimization problem can be tracked while satisfying joint limits, input limits, and without colliding into any obstacles.

ARMOUR's planning algorithm is summarized in Algorithm 4. Note in particular, that the construction and solving of the optimization problem described in lines (126) – (133) is given t_p time. If a solution is not found within that time, then the output of Algorithm 4 is set to NaN.

To facilitate real-time motion planning, we take steps to ensure that we can solve the optimization problem as quickly as possible. We therefore include the analytical constraint gradients when numerically solving the optimization problem. As described above, each constraint contains a polynomial

Algorithm 4:

```

1: Parfor  $i = 1 : N_t$ 
2:    $\{\mathbf{q}(\mathbf{T}_i; \mathbf{K}), \dots, \ddot{\mathbf{q}}_d(\mathbf{T}_i; \mathbf{K})\} \leftarrow \mathbb{PZ}(q_{d0}, \dot{q}_{d0}, \ddot{q}_{d0})$  // Sec. IX-A
3:    $\mathbf{q}_A(\mathbf{T}_i; \mathbf{K}) \leftarrow \{\mathbf{q}(\mathbf{T}_i; \mathbf{K}), \dots, \ddot{\mathbf{q}}_d(\mathbf{T}_i; \mathbf{K})\}$  // Sec. VIII-B3
4:   // create forward occupancy reachable set //
5:    $\mathbf{FK}(\mathbf{q}(\mathbf{T}_i; \mathbf{K})) \leftarrow \mathbb{PZFK}(\mathbf{q}(\mathbf{T}_i; \mathbf{K}))$  // Alg. 2
6:    $\mathbf{FO}(\mathbf{q}(\mathbf{T}_i; \mathbf{K})) \leftarrow (91)$ 
7:   // create input reachable set //
8:    $\boldsymbol{\tau}(\mathbf{q}_A(\mathbf{T}_i; \mathbf{K}), \Delta_0) \leftarrow \text{PZRNEA}(\mathbf{q}_A(\mathbf{T}_i; \mathbf{K}), \Delta_0)$  // Alg. 3
9:    $\mathbf{v}(\mathbf{q}_A(\mathbf{T}_i; \mathbf{K}), \Delta_0, [\Delta]) \leftarrow (101)$ 
10:   $\mathbf{u}(\mathbf{q}_A(\mathbf{T}_i; \mathbf{K}), \Delta_0, [\Delta]) \leftarrow (102)$ 
11:  // create constraints //
12:   $\text{jointCons}(\mathbf{q}(\mathbf{T}_i; \mathbf{K}), \dot{\mathbf{q}}(\mathbf{T}_i; \mathbf{K}))$  // Sec. IX-B1
13:   $\text{collisionCons}(\mathbf{FO}(\mathbf{q}(\mathbf{T}_i; \mathbf{K})), \mathcal{O})$  // Sec. IX-B2
14:   $\text{inputCons}(\mathbf{u}(\mathbf{T}_i; \mathbf{K}))$  // Sec. IX-B3
15: End Parfor
16: Try:  $k^* \leftarrow \text{solve } (105) - (133)$ 
17: Catch: (if  $t_e > t_p$ ), then  $k^* = \text{NaN}$  //  $t_e$  measures the amount
    of time since  $\text{Opt}$  was called //

```

Algorithm 5: ARMOUR Online Planning and Control

```

1: Require:  $t_p > 0$ ,  $N_t \in \mathbb{N}$ ,  $[\Delta]$ ,  $\Delta_0 \in [\Delta]$ ,  $\mathcal{O}$ , and  $\text{cost} : K \rightarrow \mathbb{R}$ ,
2: Initialize:  $j = 0$ ,  $t_j = 0$ , and
    $\{k_j^*\} = \text{Opt}(q_{\text{start}}, 0, 0, \mathcal{O}, \text{cost}, t_p, N_t, \Delta_0, [\Delta])$ 
3: If  $k_j^* = \text{NaN}$ , then break
4: Loop:
5:   // Line 6 executes simultaneously with Lines 7 – 9 //
6:   // Use Thm. 12, Lem. 15, and Alg. 1 //
   Apply  $u(q_A^j(t; k_j^*), \Delta_0, [\Delta])$  to robot for  $t \in [t_j, t_j + t_p]$ 
7:    $\{k_{j+1}^*\} = \text{Opt}(q_d(t_p; k_j^*), \dot{q}_d^j(t_p; k_j^*), \ddot{q}_d^j(t_p; k_j^*), \mathcal{O},$ 
      $\text{cost}, t_p, N_t, \Delta_0, [\Delta])$  // Alg. 4
8:   If  $k_{j+1}^* = \text{NaN}$ , then break
9:   Else  $t_{j+1} \leftarrow t_j + t_p$  and  $j \leftarrow j + 1$ 
10: End
11: Apply  $u(q_A^j(t; k_j^*), \Delta_0, [\Delta])$  to robot for  $t \in [t_j + t_p, t_j + t_t]$ 

```

zonotope whose coefficients correspond to the trajectory parameters and are also the decision variables of the optimization problem. Because each polynomial zonotope can be viewed as a polynomial function solely of the trajectory parameters, we can compute each constraint gradient with respect to the trajectory parameter k using the standard rules of differential calculus, *i.e.*, the power, product, and chain rules.

D. ARMOUR's Online Operation

Algorithm 5 summarizes the online operation of ARMOUR. In particular, ARMOUR uses the robust passivity-based controller (51) to track the trajectory parameter computed at the previous planning iteration on Line 6. While this input is being applied, ARMOUR computes the trajectory to be tracked at the next planning iteration on Line 7. Finally, by applying Corollary 13 and Lemma 22, one can prove that ARMOUR generates dynamically feasible, collision free behavior:

Lemma 23 (ARMOUR is Safe). *If q_{start} is collision free and one applies ARMOUR, as described in Algorithm 5, then the robot is collision free.*

We conclude by making a remark about applying ARMOUR to real-world systems. In practice, the robust passivity-based

controller on Line 6 is computed at discrete time instances at the input sampling rate requested by the robot. As we describe in Section X, the input sampling rate of manipulator robots are typically a kilohertz or more [55], [56]. Fortunately, the robust passivity-based controller can be computed at that rate. However, the input applied into the robot is usually zero-order held between sampling instances. To apply Corollary 13 in this instance, one would need to show that the tracking error bound was still satisfied if the input was applied in this zero-order held fashion. Note, one could extend the results in this paper to address this additional requirement by extending the controller presented in this paper to deal with arbitrary bounded input disturbances [53, (1)]. However, this extension falls out of the scope of this paper.

X. DEMONSTRATIONS

We now demonstrate ARMOUR in simulation and on hardware using the Kinova Gen3 7 DOF robotic arm. Our code can be found here: <https://github.com/roahmlab/armour-dev>.

A. Implementation Details

ARMOUR is implemented in MATLAB, C++, and CUDA on a desktop with a 16 core 32 thread processor, 128 GB RAM, and Nvidia Quadro RTX 8000 GPU.

1) *Kinova Robot*: The Kinova Gen3 is composed of 7 revolute DOFs [55]. During the simulation evaluation, we use the Kinova arm without its gripper. We sampled millions of configurations of the Kinova robot without gripper, and found that the minimum and maximum eigenvalues of its mass matrix were uniformly bounded from below by $\sigma_m = 5.09562$ and above by $\sigma_M = 15.79636$. We consider two setups for adding uncertainty to the inertial parameters of the arm. In the first case, we allow the mass of each link of the robot to vary by $\pm 3\%$ of its nominal value. The inertia matrices of each link vary accordingly. We refer to this setup as the “standard” set of inertial parameters, denoted by $[\Delta]$.

In the second case, we rigidly attach a 2 lb dumbbell to the arm’s end effector. The geometry of the dumbbell is considered when checking for collisions. We treat the dumbbell’s inertia as a point mass located at its centroid, and allow its mass to vary by $\pm 3\%$, without varying the rest of the arm’s parameters. We call this the “dumbbell” set of inertial parameters, denoted by $[\Delta]_{db}$.

2) *Planning Times and Trajectories*: We let $t_p = 0.5s$, and $t_f = 1s$. As in (117), we let $\eta_{j,2} = q_{d,j_0}$ and $\eta_{j,1} = \frac{\pi}{24}$, so that after $t_f = 1s$ the final position of any joint’s trajectory can differ from its initial position by up to $\pm \frac{\pi}{24}$ radians for the “standard” inertial parameters $[\Delta]$, and $\pm \frac{\pi}{50}$ radians for the “dumbbell” inertial parameters $[\Delta]_{db}$.

3) *Controller*: For the nominal passivity-based controller we set $K_r = 10I_7$, where I_7 is a 7×7 identity matrix. During our experiments, we were able to compute the passivity-based control input at approximately 15kHz. However, the software for the arm only required a control update at 1kHz.

For the robust controller, several additional parameters must be specified. As in (95), we set $\alpha(y) = y$, which satisfies the

requirement that $\alpha : \mathbb{R} \rightarrow \mathbb{R}$ is an extended class \mathcal{K}_∞ function (i.e., $\alpha : \mathbb{R} \rightarrow \mathbb{R}$ is strictly increasing with $\alpha(0) = 0$ and is defined on the entire real line $\mathbb{R} = (-\infty, \infty)$). We let the Lyapunov function threshold be $V_M = 1 \times 10^{-4}$. When we run the experiment in simulation, we do it without the gripper and the uniform bound is:

$$\varepsilon = \sqrt{\frac{2V_M}{\sigma_m}} = \sqrt{\frac{2 \times 1 \times 10^{-4}}{5.09562}} \approx 0.0062649. \quad (134)$$

Plugging into the position (68) and velocity (69) bounds yields $\varepsilon_{p,j} \approx 0.0049$ rad and $\varepsilon_v \approx 0.09818$ rad/s.

4) *Polynomial Zonotopes*: Our implementation of polynomial zonotopes and their arithmetic builds on the CORA toolbox [57]. In this work, we use a maximum zonotope order of 40, which means for 3-dimensional polynomial zonotopes a maximum of 120 generators are kept after each operation.

5) *High-level Planners*: In each planning iteration, ARMOUR minimizes a user-specified cost subject to the constraints detailed in Sec. VIII. In this work, we specify the cost as minimizing the distance between $q_d(t_f; k)$ and an intermediate waypoint q_{des} . We use high-level planners to construct these intermediate waypoints, which form a rough path to the global goal. We emphasize that ARMOUR is independent of the high-level planner, which is only used for the cost function. In fact, ARMOUR enforces safety even if the high-level planner’s waypoints are in collision or not dynamically feasible. In the majority of simulations presented here, we use a straight line high-level planner that generates waypoints along a straight line (in configuration space) between the start and goal configurations. For some scenarios (detailed below), we also test an RRT* [7] that only ensures the robot’s end effector is collision free.

6) *Comparisons*: We compare ARMOUR to a previous version of the method ARMTD [3] by running the algorithms on identical random worlds with the same high-level planner. We also compare ARMOUR to CHOMP [9] (run via MoveIt [58]) as was done previously with ARMTD. Although CHOMP is not a receding-horizon planner, it provides a useful baseline for measuring the difficulty of the scenarios encountered by ARMOUR.

7) *Algorithm Implementation*: We solve ARMOUR’s trajectory optimization using Ipopt [59]. The cost function is $\text{cost}(k) = \|q_d(t_f; k) - q_{des}\|$, where q_{des} is the intermediate waypoint provided by the high-level planner. We provide analytic gradients to the optimization solver to speed computation.

B. Simulation

1) *Setup*: As in [3], we test ARMOUR on two sets of scenes. The first set, Random Obstacles, shows that ARMOUR can handle arbitrary tasks. This set contains 100 tasks with random (but collision-free) start and goal configurations, and random box-shaped obstacles. Obstacle side lengths vary from 1 to 50 cm, with 10 scenes for each $n_O = 13, 16, \dots, 37, 40$. The second set, Hard Scenarios, shows that ARMOUR guarantees safety where CHOMP converges to an unsafe trajectory. There are seven tasks in the Hard Scenarios set shown in Fig. 3. For both these sets of scenes, ARMOUR uses the “standard”

TABLE II

Results for the 100 Random Obstacles simulations. ARMTD and ARMOUR use straight-line (SL) HLPs.

Random Obstacles	% goals	% crashes
ARMTD + SL + Δ_0	76	0
CHOMP + Δ_0	87	13
(ours) ARMOUR + SL + $[\Delta]$	93	0

TABLE III

Results for the seven Hard Scenario simulations. ARMTD and ARMOUR use straight-line (SL) and RRT* HLPs. The entries are “O” for task completed, “C” for a crash, or “S” for stopping safely without reaching the goal.

Hard Scenarios	1	2	3	4	5	6	7
CHOMP + Δ_0	C	C	C	C	C	C	C
(ours) ARMOUR + SL + $[\Delta]$	S	S	S	S	S	S	S
(ours) ARMOUR + RRT* + $[\Delta]$	O	O	O	O	O	S	O

inertial parameters $[\Delta]$ with 3% uncertainty in each link’s mass. Note that ARMOUR is compared to ARMTD and CHOMP **that are both assumed to have access to the robot’s nominal parameters Δ_0 with no uncertainty**. This should give both of these methods a considerable advantage when compared to ARMOUR.

In all tests using the Random Obstacles scenario, the straight line high-level planner is used. For the Hard Scenarios set, we also present results using the RRT*.

2) *Results:* Table II (Random Obstacles) presents ARMOUR (with a straight line high-level planner) in comparison to ARMTD and CHOMP as in [3]. ARMOUR reached 93/100 goals and had 0/100 crashes, meaning ARMOUR safely stopped in 7/100 scenes without finding a new trajectory. ARMOUR takes 398ms on average per planning iteration. Note that ARMOUR actually outperforms ARMTD using the same high-level planner despite dealing with uncertainty in the inertial parameters $[\Delta]$. This demonstrates that ARMOUR’s collision-avoidance constraints have been made less conservative than ARMTD’s. This is likely due to the updated polynomial zonotope formulation of the robot’s forward occupancy. These sets now more tightly envelop the actual reachable set of the robot, allowing for closer maneuvering around obstacles. As in [3], we note that CHOMP always finds a feasible trajectory, but not necessarily a collision-free one, as demonstrated by the 13/100 crashes. In practice, an external collision-checker can be used to verify that these trajectories are collision free before commanding them on the robot, but we note that CHOMP itself does not provide this guarantee.

Table III presents results for the Hard Scenarios. With the straight line high-level planner, ARMOUR is unable to complete any tasks but also has no collisions. With the RRT* high-level planner, ARMOUR successfully completes 6/7 scenarios and safely stops in the remaining scenario. This improves on the results for ARMTD with the same high-level planner, which completed 5/7 scenarios.

XI. CONCLUSION

We present ARMOUR, a real-time planning and control framework with strict safety guarantees for manipulators with

set-based uncertainty in their inertial parameters. A novel robust control formulation (Thm. 12) provides uniform bounds on the worst-case tracking error possible when following desired trajectories. The novel PZRNEA algorithm (Alg. 3) enables ARMOUR to compute sets of possible inputs required to track any desired trajectory, including tracking error. Polynomial zonotope arithmetic also enables the formulation of continuous-time collision-avoidance constraints. Strict joint limit, torque limit, and collision-avoidance constraints are implemented within a nonlinear program. This nonlinear program is solved at every iteration of ARMOUR’s receding-horizon planning scheme. By designing the inclusion of a fail-safe braking maneuver in every desired trajectory, ARMOUR guarantees the safe operation of the robotic arm for all time.

Several avenues of future research to improve ARMOUR are available. First, ARMOUR uses high-level planners to formulate the cost function found in ARMOUR’s optimization program. Replacing the high-level planner with one that more effectively incorporates information about the task or environment could improve ARMOUR’s success rate. Second, in this work we assume that grasped objects are rigidly attached to the robot. Future work can relax this assumption and utilize ARMOUR to reason directly over contact forces. Third, the current trajectory parameterization is sufficient for the experiments performed in this paper. However, a more calculated selection of the trajectories’ hyperparameters could reduce the time it takes ARMOUR to reach a goal. Finally, ARMOUR can be generalized by including perception within the framework, relaxing the strict safety guarantees so that they instead satisfy some acceptable measure of risk, and applying ARMOUR to different robot morphologies.

REFERENCES

- [1] A. De Luca and L. Ferrajoli, “A modified newton-euler method for dynamic computations in robot fault detection and control,” in *2009 IEEE International Conference on Robotics and Automation*, 2009, pp. 3359–3364.
- [2] N. Kochdumper and M. Althoff, “Sparse polynomial zonotopes: A novel set representation for reachability analysis,” *IEEE Transactions on Automatic Control*, vol. 66, no. 9, pp. 4043–4058, 2020.
- [3] P. Holmes, S. Kousik, B. Zhang, D. Raz, C. Barbalata, M. J. Roberson, and R. Vasudevan, “Reachable Sets for Safe, Real-Time Manipulator Trajectory Design,” in *Proceedings of Robotics: Science and Systems*, Corvallis, Oregon, USA, Jul. 2020.
- [4] E. Yoshida, I. Belousov, C. Esteves, and J.-P. Laumond, “Humanoid motion planning for dynamic tasks,” in *5th IEEE-RAS International Conference on Humanoid Robots*, 2005., IEEE, 2005, pp. 1–6.
- [5] H. Dai, A. Valenzuela, and R. Tedrake, “Whole-body motion planning with centroidal dynamics and full kinematics,” in *2014 IEEE-RAS International Conference on Humanoid Robots*, IEEE, 2014, pp. 295–302.
- [6] S. Kousik, S. Vaskov, F. Bu, M. Johnson-Roberson, and R. Vasudevan, “Bridging the gap between safety and real-time performance in receding-horizon trajectory design for mobile robots,” *The International Journal of Robotics Research*, vol. 39, no. 12, pp. 1419–1469, 2020.
- [7] S. Karaman and E. Frazzoli, “Sampling-based algorithms for optimal motion planning,” *The international journal of robotics research*, vol. 30, no. 7, pp. 846–894, 2011.
- [8] L. E. Kavraki, P. Svestka, J.-C. Latombe, and M. H. Overmars, “Probabilistic roadmaps for path planning in high-dimensional configuration spaces,” *IEEE transactions on Robotics and Automation*, vol. 12, no. 4, pp. 566–580, 1996.

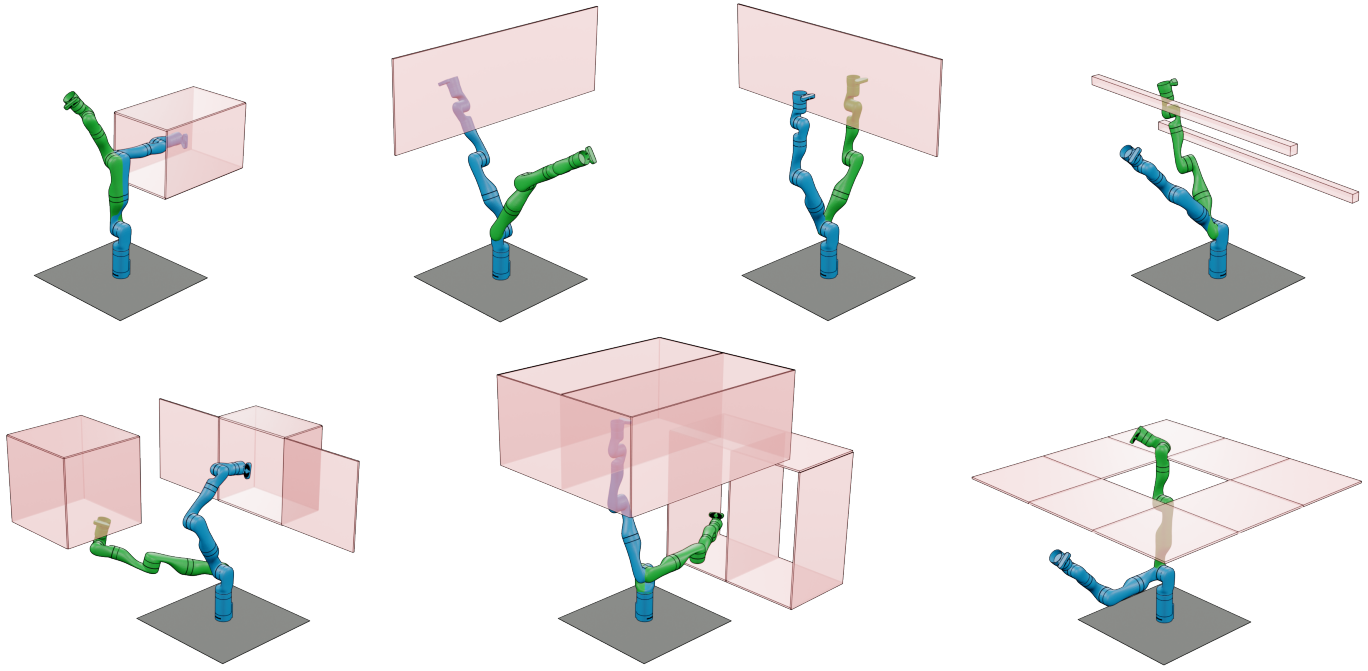


Fig. 3. The set of seven Hard Scenarios (number in the top left), with start pose shown in white and goal pose shown in black. There are seven tasks in the Hard Scenarios set: (1) from inside to outside of a box, (2-3) from one side of a wall to another, (4) between two horizontal posts, (5) from a sink to a cupboard (6) from one set of shelves to another, (7) through a small window.

- [9] M. Zucker, N. Ratliff, A. D. Dragan, M. Pivtoraiko, M. Klingensmith, C. M. Dellin, J. A. Bagnell, and S. S. Srinivasa, "Chomp: Covariant hamiltonian optimization for motion planning," *The International Journal of Robotics Research*, vol. 32, no. 9-10, pp. 1164–1193, 2013.
- [10] J. Schulman, Y. Duan, J. Ho, A. Lee, I. Awwal, H. Bradlow, J. Pan, S. Patil, K. Goldberg, and P. Abbeel, "Motion planning with sequential convex optimization and convex collision checking," *The International Journal of Robotics Research*, vol. 33, no. 9, pp. 1251–1270, 2014.
- [11] M. Elbanhawi and M. Simic, "Sampling-based robot motion planning: A review," *Ieee access*, vol. 2, pp. 56–77, 2014.
- [12] Z. Kingston, M. Moll, and L. E. Kavraki, "Sampling-based methods for motion planning with constraints," *Annual review of control, robotics, and autonomous systems*, vol. 1, pp. 159–185, 2018.
- [13] M. Kalakrishnan, S. Chitta, E. Theodorou, P. Pastor, and S. Schaal, "Stomp: Stochastic trajectory optimization for motion planning," in *2011 IEEE international conference on robotics and automation*, IEEE, 2011, pp. 4569–4574.
- [14] L. Jaillet and J. M. Porta, "Path planning under kinematic constraints by rapidly exploring manifolds," *IEEE Transactions on Robotics*, vol. 29, no. 1, pp. 105–117, 2012.
- [15] J. M. Porta, L. Jaillet, and O. Bohigas, "Randomized path planning on manifolds based on higher-dimensional continuation," *The International Journal of Robotics Research*, vol. 31, no. 2, pp. 201–215, 2012.
- [16] I. A. Sucan and S. Chitta, "Motion planning with constraints using configuration space approximations," in *2012 IEEE/RSJ International Conference on Intelligent Robots and Systems*, IEEE, 2012, pp. 1904–1910.
- [17] D. Berenson, S. S. Srinivasa, D. Ferguson, and J. J. Kuffner, "Manipulation planning on constraint manifolds," in *2009 IEEE international conference on robotics and automation*, IEEE, 2009, pp. 625–632.
- [18] S. M. Lavalle and R. Sharma, "On motion planning in changing, partially predictable environments," *The International Journal of Robotics Research*, vol. 16, no. 6, pp. 775–805, 1997.
- [19] D. Beckert, A. Pereira, and M. Althoff, "Online verification of multiple safety criteria for a robot trajectory," in *2017 IEEE 56th Annual Conference on Decision and Control (CDC)*, IEEE, 2017, pp. 6454–6461.
- [20] L. Scalera, R. Vidoni, and A. Giusti, "Optimal scaling of dynamic safety zones for collaborative robotics," in *2021 IEEE International Conference on Robotics and Automation (ICRA)*, IEEE, 2021, pp. 3822–3828.
- [21] L. Scalera, A. Giusti, R. Vidoni, and A. Gasparetto, "Online planning of path-consistent stop trajectories for collaborative robotics," in *The International Conference of IFTOMM ITALY*, Springer, 2022, pp. 693–701.
- [22] J. J. Kuffner, S. Kagami, K. Nishiwaki, M. Inaba, and H. Inoue, "Dynamically-stable motion planning for humanoid robots," *Autonomous robots*, vol. 12, no. 1, pp. 105–118, 2002.
- [23] F. Kanehiro, W. Suleiman, F. Lamiroux, E. Yoshida, and J.-P. Laumond, "Integrating dynamics into motion planning for humanoid robots," in *2008 IEEE/RSJ International Conference on Intelligent Robots and Systems*, IEEE, 2008, pp. 660–667.
- [24] Y. Han, R. Li, and G. S. Chirikjian, "Can i lift it? humanoid robot reasoning about the feasibility of lifting a heavy box with unknown physical properties," in *2020 IEEE/RSJ International Conference on Intelligent Robots and Systems (IROS)*, IEEE, 2020, pp. 3877–3883.
- [25] N. D. Ratliff, J. Issac, D. Kappler, S. Birchfield, and D. Fox, "Riemannian motion policies," *arXiv preprint arXiv:1801.02854*, 2018.
- [26] A. Bylard, R. Bonalli, and M. Pavone, "Composable geometric motion policies using multi-task pullback bundle dynamical systems," *arXiv e-prints*, arXiv:2101, 2021.
- [27] S. S. M. Salehian, N. Figueroa, and A. Billard, "Coordinated multi-arm motion planning: Reaching for moving objects in the face of uncertainty," in *Proceedings of Robotics: Science and Systems*, Ann Arbor, Michigan, Jun. 2016.
- [28] M. Koptev, N. Figueroa, and A. Billard, "Real-time self-collision avoidance in joint space for humanoid robots," *IEEE Robotics and Automation Letters*, vol. 6, no. 2, pp. 1240–1247, 2021.
- [29] C. Abdallah, D. M. Dawson, P. Dorato, and M. Jamshidi, "Survey of robust control for rigid robots," *IEEE Control Systems Magazine*, vol. 11, no. 2, pp. 24–30, 1991.
- [30] H. Sage, M. De Mathelin, and E. Ostertag, "Robust control of robot manipulators: A survey," *International Journal of control*, vol. 72, no. 16, pp. 1498–1522, 1999.
- [31] J.-J. Slotine and S. S. Sastry, "Tracking control of non-linear systems using sliding surfaces, with application to robot manipulators," *International journal of control*, vol. 38, no. 2, pp. 465–492, 1983.
- [32] J.-J. E. Slotine, "The robust control of robot manipulators," *The International Journal of Robotics Research*, vol. 4, no. 2, pp. 49–64, 1985.

- [33] S. Islam and X. P. Liu, “Robust sliding mode control for robot manipulators,” *IEEE Transactions on industrial electronics*, vol. 58, no. 6, pp. 2444–2453, 2010.
- [34] M. B. R. Neila and D. Tarak, “Adaptive terminal sliding mode control for rigid robotic manipulators,” *International Journal of Automation and Computing*, vol. 8, no. 2, pp. 215–220, 2011.
- [35] J. Baek, M. Jin, and S. Han, “A new adaptive sliding-mode control scheme for application to robot manipulators,” *IEEE Transactions on industrial electronics*, vol. 63, no. 6, pp. 3628–3637, 2016.
- [36] M. Zhu, L. Ye, and X. Ma, “Estimation-based quadratic iterative learning control for trajectory tracking of robotic manipulator with uncertain parameters,” *IEEE Access*, vol. 8, pp. 43 122–43 133, 2020.
- [37] A. Giusti and M. Althoff, “Efficient computation of interval-arithmetic-based robust controllers for rigid robots,” in *2017 First IEEE International Conference on Robotic Computing (IRC)*, IEEE, 2017, pp. 129–135.
- [38] M. Wagner, S. Liu, A. Giusti, and M. Althoff, “Interval-arithmetic-based trajectory scaling and collision detection for robots with uncertain dynamics,” in *2018 Second IEEE International Conference on Robotic Computing (IRC)*, IEEE, 2018, pp. 41–48.
- [39] A. Giusti, S. B. Liu, and M. Althoff, “Interval-arithmetic-based robust control of fully actuated mechanical systems,” *IEEE Transactions on Control Systems Technology*, Oct. 2021.
- [40] S. Malan, M. Milanese, and M. Taragna, “Robust analysis and design of control systems using interval arithmetic,” *Automatica*, vol. 33, no. 7, pp. 1363–1372, 1997.
- [41] Y. Smagina and I. Brewer, “Using interval arithmetic for robust state feedback design,” *Systems & Control Letters*, vol. 46, no. 3, pp. 187–194, 2002.
- [42] L. Jaulin, “Nonlinear bounded-error state estimation of continuous-time systems,” *Automatica*, vol. 38, no. 6, pp. 1079–1082, 2002.
- [43] J. M. Bravo, D. Limón, T. Alamo, and E. F. Camacho, “On the computation of invariant sets for constrained nonlinear systems: An interval arithmetic approach,” *Automatica*, vol. 41, no. 9, pp. 1583–1589, 2005.
- [44] T. Hickey, Q. Ju, and M. H. Van Emden, “Interval arithmetic: From principles to implementation,” *Journal of the ACM (JACM)*, vol. 48, no. 5, pp. 1038–1068, 2001.
- [45] M. Althoff, “Reachability analysis and its application to the safety assessment of autonomous cars,” Ph.D. dissertation, Technische Universität München, 2010.
- [46] L. J. Guibas, A. Nguyen, and L. Zhang, “Zonotopes as bounding volumes,” in *Proceedings of the fourteenth annual ACM-SIAM symposium on Discrete algorithms*, Society for Industrial and Applied Mathematics, 2003, pp. 803–812.
- [47] M. Althoff, “Reachability analysis of nonlinear systems using conservative polynomialization and non-convex sets,” in *Proceedings of the 16th international conference on Hybrid systems: computation and control*, 2013, pp. 173–182.
- [48] T. M. Apostol, *Calculus, Volume 1*. John Wiley & Sons, 1991.
- [49] M. Spong, S. Hutchinson, and M. Vidyasagar, “Robot modeling and control,” 2005.
- [50] S. Vaskov, S. Kousik, H. Larson, F. Bu, J. R. Ward, S. Worrall, M. Johnson-Roberson, and R. Vasudevan, “Towards provably not-at-fault control of autonomous robots in arbitrary dynamic environments,” in *Proceedings of Robotics: Science and Systems*, Freiburg/Breisgau, Germany, Jun. 2019.
- [51] S. Kousik, P. Holmes, and R. Vasudevan, “Safe, aggressive quadrotor flight via reachability-based trajectory design,” in *Dynamic Systems and Control Conference*, American Society of Mechanical Engineers, vol. 59162, 2019, V003T19A010.
- [52] J. Liu, Y. Shao, L. Lymburner, H. Qin, V. Kaushik, L. Trang, R. Wang, V. Ivanovic, H. E. Tseng, and R. Vasudevan, “Refine: Reachability-based trajectory design using robust feedback linearization and zonotopes,” *arXiv preprint arXiv:2211.11997*, 2022.
- [53] A. Giusti and M. Althoff, “Ultimate robust performance control of rigid robot manipulators using interval arithmetic,” in *2016 American Control Conference (ACC)*, 2016, pp. 2995–3001.
- [54] C. C. de Wit, B. Siciliano, and G. Bastin, *Theory of robot control*. Springer Science & Business Media, 2012.
- [55] Kinova, *User Guide - KINOVA Gen3 Ultra lightweight robot*. 2022.
- [56] Franka, *User Guide - PANDA - DATASHEET*. 2019.
- [57] M. Althoff, “An Introduction to CORA 2015,” in *Proc. of the Workshop on Applied Verification for Continuous and Hybrid Systems*, 2015.
- [58] D. Coleman, I. A. Sucan, S. Chitta, and N. Correll, “Reducing the Barrier to Entry of Complex Robotic Software: a MoveIt! Case Study,” *CoRR*, vol. abs/1404.3785, 2014.
- [59] A. Wächter and L. Biegler, “On the implementation of an interior-point filter line-search algorithm for large-scale nonlinear programming,” *Mathematical programming*, vol. 106, pp. 25–57, Mar. 2006.
- [60] R. Konda, A. D. Ames, and S. Coogan, “Characterizing safety: Minimal control barrier functions from scalar comparison systems,” *IEEE Control Systems Letters*, vol. 5, no. 2, pp. 523–528, 2020.
- [61] B. Siciliano, L. Sciacivico, L. Villani, and G. Oriolo, “Modelling, planning and control,” *Advanced Textbooks in Control and Signal Processing*. Springer, 2009.

APPENDIX A PROOF OF THM. 12

Proof. To begin, let

$$h(q_A(t), \Delta) = -V(q_A(t), \Delta) + V_M. \quad (135)$$

This proof shows that h is a minimal Control Barrier Function (CBF) under the control input (65) [60, Definition 3]. If we prove this property and show that the control input (65) is continuous with respect to its first argument, then all zero super-level sets of h , which are defined as

$$H = \{q_A(t) \mid h(q_A(t), \Delta) \geq 0\}, \quad (136)$$

are forward invariant [60, Theorem 4].

If H is forward invariant, this proves the desired bound on $r(t)$ for all $t \in T$. To see this, first recall that $r(0) = 0$ because $e(0) = \dot{e}(0) = 0$ by hypothesis. When the value of $q_A(0)$ associated with this $r(0)$ is plugged into h , we get that $q_A(0) \in H$ because $V_M > 0$. This implies that at $t = 0$, the trajectory begins within H and as a result will remain in H if the system is forward invariant. Next, note $h(q_A(t), \Delta) \geq 0, \forall q_A(t) \in H$. This implies that $V(q_A(t), \Delta) \leq V_M, \forall q_A(t) \in H$. Note that $V(q_A(t), \Delta)$ can be lower bounded using the uniform minimum eigenvalue σ_m according to Assumption 11:

$$\frac{1}{2} \sigma_m \|r(t)\|^2 \leq \frac{1}{2} r(t)^\top M(q(t), \Delta) r(t) = V(q_A(t), \Delta). \quad (137)$$

Therefore, we have $\frac{1}{2} \sigma_m \|r(t)\|^2 \leq V_M$, which gives

$$\|r(t)\| \leq \varepsilon \quad \forall q_A(t) \in H. \quad (138)$$

As a result, all that remains to show is that 1. h is a minimal control barrier function and 2. the robust control (65) is continuous.

Proving that h is a minimal CBF: Recall that rigid body robot dynamics as in our manipulator dynamics can be written in control affine form [49, (6.61)]. As a result, to prove that h is a minimal control barrier function, we need to prove that the following condition is satisfied under the robust control input:

$$\dot{h}(q_A(t)) \geq -\alpha(h(q_A(t), \Delta)). \quad (139)$$

Note that to apply [60, Definition 3] α must be a minimal function, but any extended class \mathcal{K}_∞ function is a minimal one [60, Case 2, Theorem 2]. As we show below, \dot{h} is a function of Δ, Δ_0 , and $[\Delta]$. However, because these dependencies are clear in context we suppress them for convenience.

Before proving this result, we make several observations: First, the Lyapunov function V is positive definite because

$M(q(t), \Delta)$ is positive definite. Second, a suitable factorization of $C(q(t), \dot{q}(t), \Delta)$ renders the matrix $N(q(t), \dot{q}(t), \Delta) = \dot{M}(q(t), \Delta) - 2C(q(t), \dot{q}(t), \Delta)$ skew-symmetric [61, Ch. 7]. Therefore,

$$x^\top N(q(t), \dot{q}(t), \Delta)x = 0, \quad \forall x \in \mathbb{R}^{n_q}. \quad (140)$$

Taking the derivative of $V(q_A(t), \Delta)$ with respect to time, we obtain

$$\begin{aligned} \dot{V}(q_A(t)) &= r(t)^\top M(q(t), \Delta) \dot{r}(t) + \\ &\quad + \frac{1}{2} r(t)^\top \dot{M}(q(t), \Delta) r(t), \end{aligned} \quad (141)$$

which after substituting (57) and taking advantage of (140) yields

$$\begin{aligned} \dot{V}(q_A(t)) &= r(t)^\top v(q_A(t), \Delta_0, [\Delta]) + \\ &\quad + r(t)^\top w(q_A(t), \Delta_0, \Delta). \end{aligned} \quad (142)$$

Note, \dot{V} is a function of Δ, Δ_0 , and $[\Delta]$, but we have suppressed these dependencies for convenience. As a result,

$$\dot{h}(q_A(t)) = -\dot{V}(q_A(t)) \quad (143)$$

$$= -r(t)^\top v(q_A(t), \Delta_0, [\Delta]) + \quad (144)$$

$$-r(t)^\top w(q_A(t), \Delta_0, \Delta), \quad (145)$$

so (139) becomes

$$\begin{aligned} -r(t)^\top v(q_A(t), \Delta_0, [\Delta]) + \\ -r(t)^\top w(q_A(t), \Delta_0, \Delta) \geq -\alpha(h(q_A(t), \Delta)). \end{aligned} \quad (146)$$

Our task is to choose v so that (146) is always satisfied.

As a consequence of Lem. 10 and (63), $|r(t)|^\top w_M(q_A(t), \Delta_0, [\Delta]) \geq r(t)^\top w(q_A(t), \Delta_0, \Delta)$, and therefore we can rearrange (146) to obtain the stricter condition:

$$\begin{aligned} -r(t)^\top v(q_A(t), \Delta_0, [\Delta]) \geq -\alpha(h(q_A(t), \Delta)) + \\ + |r(t)|^\top w_M(q_A(t), \Delta_0, [\Delta]), \end{aligned} \quad (147)$$

whose satisfaction guarantees that (146) is also satisfied. Notice that the left hand side expression is maximized when $v(q_A(t), \Delta_0, [\Delta])$ points in the $-\frac{r(t)}{\|r(t)\|}$ direction. Therefore, we choose $v(q_A(t), \Delta_0, [\Delta]) = -\gamma(q_A(t), \Delta_0, [\Delta]) \frac{r(t)}{\|r(t)\|}$, where $\gamma(q_A(t), \Delta_0, [\Delta]) \geq 0$ is a non-negative scalar, which yields

$$\begin{aligned} \gamma(q_A(t), \Delta_0, [\Delta]) \|r(t)\| \geq -\alpha(h(q_A(t), \Delta)) + \\ + |r(t)|^\top w_M(q_A(t), \Delta_0, [\Delta]). \end{aligned} \quad (148)$$

Choosing $\gamma(q_A(t), \Delta_0, [\Delta]) \geq 0$ and

$$\gamma(q_A(t), \Delta_0, [\Delta]) \geq \frac{-\alpha(h(q_A(t), \Delta)) + |r(t)|^\top w_M(q_A(t), \Delta_0, [\Delta])}{\|r(t)\|} \quad (149)$$

ensures that condition (139) is satisfied and $h(q_A(t), \Delta)$ is a minimal CBF.

However, this choice of γ requires the value $h(q_A(t), \Delta)$. Because we do not know the true inertial parameters Δ , we can not exactly compute $M(q(t), \Delta)$ which is required to find $h(q_A(t), \Delta)$. Instead, we can bound these values over the range of inertial parameters. Given a particular $q_A(t)$, $\underline{h}(q_A(t), [\Delta])$ as in (62) lower bounds $h(q_A(t), \Delta)$ because $\Delta \in [\Delta]$. The inequality $\underline{h}(q_A(t), [\Delta]) \leq h(q_A(t), \Delta)$ implies

that $-\alpha(\underline{h}(q_A(t), [\Delta])) \geq -\alpha(h(q_A(t), \Delta))$; therefore, choosing $\gamma(q_A(t), \Delta_0, [\Delta]) \geq 0$ and

$$\gamma(q_A(t), \Delta_0, [\Delta]) \geq \frac{-\alpha(\underline{h}(q_A(t), [\Delta])) + |r(t)|^\top w_M(q_A(t), \Delta_0, [\Delta])}{\|r(t)\|} \quad (150)$$

ensures that condition (139) is satisfied and h is a minimal CBF. The γ in (66) satisfies these conditions.

Proving that the robust control (65) is continuous: Note that the robust control input could only be discontinuous when $\|r(t)\| = 0$. We will prove that for all points in a neighborhood of the point $\|r(t)\| = 0$, $\gamma(q_A(t), \Delta_0, [\Delta]) = 0$ where Δ_0 and $[\Delta]$ are held fixed. If we prove this result, then the desired result follows.

Before proceeding further, recall from Assumption 11 that there exists a finite $\sigma_M > 0$ on the largest eigenvalue of $M(q(t), \Delta)$, and therefore

$$-\frac{1}{2} r(t)^\top M(q(t), \Delta) r(t) \geq -\frac{1}{2} \sigma_M \|r(t)\|^2 \quad (151)$$

for all $\Delta \in [\Delta]$ and $q(t) \in \mathcal{Q}$. Next, note that there exists $r_M \geq 0$ such that for all $r(t)$ with $\|r(t)\| \leq r_M$, we have $-\frac{1}{2} \sigma_M \|r(t)\|^2 + V_M > 0$. This implies that there exists some $\zeta > 0$ such that $\underline{h}(q_A(t), [\Delta]) > \zeta$ for all $q_A(t)$ with $\|r(t)\| \leq r_M$. Because α is an extended class \mathcal{K}_∞ function, this implies that

$$\begin{aligned} \frac{-\alpha(\underline{h}(q_A(t), [\Delta]))}{\|r(t)\|} + \frac{|r(t)|^\top w_M(q_A(t), \Delta_0, [\Delta])}{\|r(t)\|} < \frac{-\alpha(\zeta)}{\|r(t)\|} + \\ + |w_M(q_A(t), \Delta_0, [\Delta])|, \end{aligned} \quad (152)$$

where we have also used the fact that $|r(t)|^\top w_M(q_A(t), \Delta_0, [\Delta]) \leq \|r(t)\| \|w_M(q_A(t), \Delta_0, [\Delta])\|$. Because $\alpha(\zeta) > 0$, the previous inequality implies $\frac{-\alpha(\underline{h}(q_A(t), [\Delta]))}{\|r(t)\|} + |w_M(q_A(t), \Delta_0, [\Delta])| \rightarrow -\infty$ as $\|r(t)\| \rightarrow 0$. As a result, $\gamma(q_A(t), \Delta_0, [\Delta]) = 0$ for all $r(t)$ with $\|r(t)\| \leq r_M$ because of the max in (66), which proves the desired result. \square

APPENDIX B PROOF OF COR. 13

Proof. Consider (58), which we rearrange as

$$\dot{e}(t) = -K_r e(t) + r(t). \quad (153)$$

Notice that K_r is diagonal and positive definite, so this defines n_q first-order linear systems where we can treat r as an input that is bounded (i.e., $|r_j(t)| \leq \varepsilon$ as in (67)). The solution of the j^{th} system is given by

$$e_j(t) = \exp(-K_{r,j}t) e_j(0) + \int_0^t \exp(-K_{r,j}(t-s)) r_j(s) ds. \quad (154)$$

By hypothesis $e_j(0) = 0$, yielding

$$e_j(t) = \int_0^t \exp(-K_{r,j}(t-s)) r_j(s) ds. \quad (155)$$

Because of the uniform bound $|r_j(t)| \leq \varepsilon$, we obtain

$$|e_j(t)| \leq \left| \int_0^t \exp(-K_{r,j}(t-s)) \varepsilon ds \right|. \quad (156)$$

Rearranging yields

$$|e_j(t)| \leq \left| \exp(-K_{r,j}t) \varepsilon \int_0^t \exp(K_{r,j}s) ds \right|. \quad (157)$$

The definite integral can be evaluated:

$$|e_j(t)| \leq \left| \exp(-K_{r,j}t) \frac{1}{K_{r,j}} \varepsilon (\exp(K_{r,j}t) - 1) \right|. \quad (158)$$

Multiplying terms gives

$$|e_j(t)| \leq \left| \frac{1}{K_{r,j}} \varepsilon (1 - \exp(-K_{r,j}t)) \right|. \quad (159)$$

Notice that the term $\exp(-K_{r,j}t) \in [0, 1] \forall t \geq 0$, and therefore

$$|e_j(t)| \leq \frac{1}{K_{r,j}} \varepsilon \quad (160)$$

as desired.

This bound on position error yields a bound on the velocity error. From (153), we have

$$|\dot{e}_j(t)| = |-K_{r,j}e(t) + r(t)|. \quad (161)$$

Applying the triangle inequality, we obtain

$$|\dot{e}_j(t)| \leq |K_{r,j}e_j(t)| + |r_j(t)|, \quad (162)$$

and finally plugging in (160) yields

$$|\dot{e}_j(t)| \leq 2\varepsilon. \quad (163)$$

□

APPENDIX C PROOF OF LEM. 15

Proof. First, notice that because the IRNEA Algorithm is replacing all operations over the inertial parameters in the original RNEA Algorithm with interval arithmetic equivalents, we have $\text{RNEA}(q_A(t), \Delta_0, a_0^0) \in \text{IRNEA}(q_A(t), [\Delta], a_0^0)$ for $\Delta_0 \in [\Delta]$. As a result, we have $w(q_A(t), \Delta_0, \Delta) \in [w(q_A(t), \Delta_0, [\Delta])]$. The satisfaction of (63) follows.

Next, note that max, absolute value, and norm operations are all continuous functions, so if we prove that $\inf([w(q_A(t), \Delta_0, [\Delta])])$ and $\sup([w(q_A(t), \Delta_0, [\Delta])])$ are continuous in their first argument, then w_M is continuous in its first argument. To see that $\inf([w(q_A(t), \Delta_0, [\Delta])])$ and $\sup([w(q_A(t), \Delta_0, [\Delta])])$ are continuous functions of $q_A(t)$, note that $q_A(t)$ is a vector argument to IRNEA, which is used to generate a homogeneous transformation matrix as in (35). Note that the homogeneous transformation matrix is a continuous function of $q_A(t)$. Because all subsequent operations within IRNEA are either interval additions, subtractions, or matrix multiplications of the interval inertia parameters with the homogeneous transformation matrix or the velocity/acceleration vectors in $q_A(t)$, the lower or upper bound of the interval output to IRNEA is a continuous function of $q_A(t)$.

To prove the desired result for \underline{h} , first notice that if we use $q_R(t)$ in place of $q_A(t)$, then when we apply (50), we have $\dot{q}_a(t) = 0$ and $\ddot{q}_a(t) = r(t)$. As a result, because IRNEA is computing an interval version of (52) and is using interval arithmetic, we have $M(q(t), \Delta_0)r(t) \in \text{IRNEA}(q_R(t), [\Delta], 0)$ for

$\Delta_0 \in [\Delta]$. Therefore by applying the properties of interval arithmetic, the \underline{h} defined as in (76) satisfies (62). The continuity of \underline{h} in its first argument follows from an identical argument as the one made for w_M . □

APPENDIX D LEMMA 24

We provide the following lemma which is utilized in the proof of Thm. 20.

Lemma 24. *Given vectors $a, b \in \mathbb{R}^{n_q}$ of unit norm $\|a\| = \|b\| = 1$, consider the optimization problem*

$$\max_{c \in \mathbb{R}^{n_q}} f(c) \quad (164)$$

$$\|c\| = 1 \quad (165)$$

where $f(c) = (a^\top c)(b^\top c)$ is the product of the dot products of a and b with c . At the optimal solution c^* , the cost $f(c^*)$ is given by

$$f(c^*) = \frac{1 + a^\top b}{2}. \quad (166)$$

Proof. Consider the scalar quantity $(a^\top c - b^\top c)^2$. We know that $(a^\top c - b^\top c)^2 \geq 0$, and expanding the left hand side yields $(a^\top c)^2 - 2(a^\top c)(b^\top c) + (b^\top c)^2 \geq 0$. Adding $4(a^\top c)(b^\top c)$ to both sides yields $(a^\top c)^2 + 2(a^\top c)(b^\top c) + (b^\top c)^2 \geq 4(a^\top c)(b^\top c)$, which gives $(a^\top c + b^\top c)^2 \geq 4(a^\top c)(b^\top c)$. Therefore, we have

$$f(c) \leq \frac{(a^\top c + b^\top c)^2}{4}. \quad (167)$$

Note that if $a^\top c = b^\top c$, (167) actually becomes an equality.

Restating (167) using the distributive property gives

$$f(c) \leq \frac{((a+b)^\top c)^2}{4}. \quad (168)$$

The right hand side is maximized when c points in the $a+b$ direction, so we choose $c^* = \frac{(a+b)}{\|a+b\|}$. Plugging in, we obtain

$$f(c^*) \leq \frac{((a+b)^\top \frac{(a+b)}{\|a+b\|})^2}{4}. \quad (169)$$

Note that $\|a+b\|^2 = (a+b)^\top (a+b)$, and therefore

$$f(c^*) \leq \frac{((a+b)^\top (a+b))^2}{4(a+b)^\top (a+b)}. \quad (170)$$

Cancelling terms, multiplying, and using the fact that $a^\top a = b^\top b = 1$, we obtain

$$f(c^*) \leq \frac{1 + a^\top b}{2}. \quad (171)$$

Finally, note that $a^\top c^* = b^\top c^* = \frac{1 + a^\top b}{\|a+b\|}$, and thus equality holds in (167). Therefore, we have

$$f(c^*) = \frac{1 + a^\top b}{2} \quad (172)$$

as desired. □

APPENDIX E
PROOF OF THM. 20

Proof. We seek a bound on the magnitude of the j^{th} component of the robust input vector (65). For notation convenience throughout this proof, we drop the dependence on k in q_A and r . From (65) we have that

$$|v(q_A(t), \Delta_0, [\Delta])_j| = \gamma(q_A(t), \Delta_0, [\Delta]) \frac{|r(t)_j|}{\|r(t)\|}, \quad (173)$$

From (66), we have

$$\gamma(q_A(t), \Delta_0, [\Delta]) = \max \left(0, \frac{-\alpha(\underline{h}(q_A(t), [\Delta]))}{\|r(t)\|} + \frac{|r(t)|^\top w_M(q_A(t), \Delta_0, [\Delta])}{\|r(t)\|} \right), \quad (174)$$

If 0 achieves the maximum in the RHS of the above expression, then $\gamma(q_A(t; k), \Delta_0, [\Delta]) = 0$ and (99) holds trivially. Therefore, we bound:

$$|v(q_A(t), \Delta_0, [\Delta])_j| \leq \frac{-\alpha(\underline{h}(q_A(t), [\Delta]))}{\|r(t)\|} \frac{|r(t)_j|}{\|r(t)\|} + \frac{|r(t)|^\top w_M(q_A(t), \Delta_0, [\Delta])}{\|r(t)\|} \frac{|r(t)_j|}{\|r(t)\|}. \quad (175)$$

In the RHS of the above inequality, note that the first term is negative when $\underline{h}(q_A(t), [\Delta]) > 0$, and that the second term is always positive (because all elements of $w_M(q_A(t), \Delta_0, [\Delta])$ are ≥ 0 by (63)). The RHS is therefore largest when $\underline{h}(q_A(t), [\Delta])$ is as negative as possible, so we examine this case when searching for a bound.

First, we seek an upper bound on $\frac{-\alpha(\underline{h}(q_A(t), [\Delta]))}{\|r(t)\|} \frac{|r(t)_j|}{\|r(t)\|}$ (which occurs when $\underline{h}(q_A(t), [\Delta])$ is as negative as possible). Through the same line of reasoning which follows (151) in Appendix A, we know that $-\frac{1}{2}\sigma_M \|r(t)\|^2 + V_M \leq \underline{h}(q_A(t), [\Delta])$. Plugging in yields

$$\frac{-\alpha(\underline{h}(q_A(t), [\Delta]))}{\|r(t)\|} \frac{|r(t)_j|}{\|r(t)\|} \leq \frac{-\alpha(-\frac{1}{2}\sigma_M \|r(t)\|^2 + V_M)}{\|r(t)\|} \quad (176)$$

where we have used the fact that $|r(t)_j| \leq \|r(t)\|$. With the linear form of α defined in (95), we have

$$\frac{-\alpha(-\frac{1}{2}\sigma_M \|r(t)\|^2 + V_M)}{\|r(t)\|} = \alpha_c \frac{1}{2} \sigma_M \|r(t)\| - \alpha_c \frac{V_M}{\|r(t)\|}. \quad (177)$$

The negative sign in front of V_M means that we want to divide by as large a value of $\|r(t)\|$ as possible to make this negative quantity as small as possible to construct an upper bound. Recall that a bound on $\|r(t)\| \leq \varepsilon$ is already known from (67). With the uniform bound (64), this becomes

$$\alpha_c \frac{1}{2} \sigma_M \|r(t)\| - \alpha_c \frac{V_M}{\|r(t)\|} \leq \alpha_c \frac{1}{2} \sigma_M \varepsilon - \alpha_c \frac{V_M}{\varepsilon}, \quad (178)$$

Notice from (64) that $V_M = \frac{1}{2}\sigma_m \varepsilon^2$, and substituting gives

$$\frac{-\alpha(\underline{h}(q_A(t; k), [\Delta]))}{\|r(t)\|} \frac{|r(t; k)_j|}{\|r(t; k)\|} \leq \frac{\alpha_c \varepsilon (\sigma_M - \sigma_m)}{2}. \quad (179)$$

Next, we seek an upper bound on $\frac{|r(t)|^\top w_M(q_A(t), \Delta_0, [\Delta])}{\|r(t)\|} \frac{|r(t)_j|}{\|r(t)\|}$, which stems from the worst case disturbance. With $w_M(\star)$ as in (98), we have

$$\frac{|r(t)|^\top w_M(q_A(t), \Delta_0, [\Delta])}{\|r(t)\|} \leq \frac{|r(t)|^\top w_M(\star)}{\|r(t)\|}. \quad (180)$$

where $w_M(\star) = w_M(\mathbf{q}_A(\mathbf{T}_i; \mathbf{K}), \Delta_0, [\Delta])$ for brevity.

Bringing the norm of $w_M(\star)$ outside, we know that

$$\frac{|r(t)|^\top w_M(\star)}{\|r(t)\|} \frac{|r(t)_j|}{\|r(t)\|} = \|w_M(\star)\| \left(\frac{w_M(\star)^\top}{\|w_M(\star)\|} \frac{|r(t)|}{\|r(t)\|} \hat{z}_j^\top \frac{|r(t)|}{\|r(t)\|} \right), \quad (181)$$

where \hat{z}_j^\top is a unit vector comprised of all zeros except a 1 in the j^{th} dimension. The quantity in parentheses is a product of two dot products, where all vectors are unit vectors. Applying Lem. 24, we arrive at

$$\frac{|r(t)|^\top w_M(q_A(t), \Delta_0, [\Delta])}{\|r(t)\|} \frac{|r(t)_j|}{\|r(t)\|} \leq \frac{\|w_M(\star)\| + w_M(\star)_j}{2}. \quad (182)$$

Combining (179) and (182) with (175), we obtain

$$|v(q_A(t; k), \Delta_0, [\Delta])_j| \leq \frac{\alpha_c \varepsilon (\sigma_M - \sigma_m) + \|w_M(\star)\| + w_M(\star)_j}{2}. \quad (183)$$

□

APPENDIX F
COMPARISON OF ROBUST INPUT BOUND TO PUBLISHED WORK

ARMOUR's robust input (given in (65)) is inspired by the work of Andrea Giusti and Matthias Althoff [37], [53]. We claim that the proposed controller improves on these published controllers because it achieves the same uniform bound with a smaller robust input bound.

From [53, Thm. 1, Eq. 10], the robust input given in previous work is

$$v(q_A(t), \Delta_0, [\Delta]) = -\left(\kappa(t) \|w_M(q_A(t), \Delta_0, [\Delta])\| + \phi(t)\right) r(t), \quad (184)$$

where $\kappa(t)$ and $\phi(t)$ are positive increasing functions with $\kappa_P \geq 1$ and $\phi_P \geq 1$ as their respective minimums, and $w_M(q_A(t), \Delta_0, [\Delta])$ as in (63). With this choice of robust input, [53, Thm. 1] proves that the trajectories of r are ultimately uniformly bounded by

$$\|r(t)\| \leq \frac{1}{\kappa_P} \sqrt{\frac{\sigma_M}{\sigma_m}} \quad \forall t \geq t_1 \quad (185)$$

where t_1 is some finite time. We note that in the context of Remark 14, this bound would hold for all time if (184) were used in the current framework. This uniform bound can be made identical to (67) by choosing $\kappa_P = \sqrt{\frac{\sigma_M}{2V_M}}$, which yields

$$\frac{1}{\kappa_P} \sqrt{\frac{\sigma_M}{\sigma_m}} = \sqrt{\frac{2V_M}{\sigma_M}} \sqrt{\frac{\sigma_M}{\sigma_m}} = \sqrt{\frac{2V_M}{\sigma_m}} \quad (186)$$

as desired.

We seek a bound on the magnitude of the robust input similarly to Appendix E. We have that

$$|v(q_A(t), \Delta_0, [\Delta])_j| = \left(\kappa(t) \|w_M(q_A(t), \Delta_0, [\Delta])\| + \phi(t)\right) |r_j(t)|. \quad (187)$$

The smallest possible bound on the term $|r_j(t)|$ is given by (185), which yields $|r_j(t)| \leq \|r(t)\| \leq \frac{1}{\kappa_P} \sqrt{\frac{\sigma_M}{\sigma_m}}$. Defining $w_M(\star) = w_M(\mathbf{q}_A(\mathbf{T}_i; \mathbf{K}), \Delta_0, [\Delta])$ as in (98), we have

$$|v(q_A(t), \Delta_0, [\Delta])|_j \leq \left(\kappa(t) \|w_M(\star)\| + \phi(t) \right) \frac{1}{\kappa_P} \sqrt{\frac{\sigma_M}{\sigma_m}} \quad (188)$$

for all $t \in \mathbf{T}_i$. Next, we show that a lower bound on the right hand side of this equation (i.e. a lower bound on the robust input bound) is larger than the robust input bound (99) developed in Appendix E for ARMOUR's robust input.

Both $\kappa(t)$ and $\phi(t)$ are positive increasing functions with minimums $\kappa_P \geq 1$ and $\phi_P \geq 1$. Therefore,

$$\left(\kappa_P \|w_M(\star)\| \right) \frac{1}{\kappa_P} \sqrt{\frac{\sigma_M}{\sigma_m}} \leq \left(\kappa(t) \|w_M(\star)\| + \phi(t) \right) \frac{1}{\kappa_P} \sqrt{\frac{\sigma_M}{\sigma_m}}. \quad (189)$$

Cancelling terms on the left hand side gives

$$\|w_M(\star)\| \sqrt{\frac{\sigma_M}{\sigma_m}} \leq \left(\kappa(t) \|w_M(\star)\| + \phi(t) \right) \frac{1}{\kappa_P} \sqrt{\frac{\sigma_M}{\sigma_m}}. \quad (190)$$

To summarize, this says that the robust input bound for (184) is larger than $\|w_M(\star)\| \sqrt{\frac{\sigma_M}{\sigma_m}}$.

Finally, we compare this value to ARMOUR's robust input bound in (99). Under what conditions is the proposed robust input bound (99) smaller, i.e.

$$\frac{\alpha_c \varepsilon (\sigma_M - \sigma_m) + \|w_M(\star)\| + w_M(\star)_j}{2} \stackrel{?}{\leq} \|w_M(\star)\| \sqrt{\frac{\sigma_M}{\sigma_m}}. \quad (191)$$

This relation depends on the values of user-specified constants α_c and ε , as well as the maximum and minimum eigenvalues σ_M and σ_m , but generally the following are true. First, $\sigma_M \geq \sigma_m$ by definition, and usually σ_M is much larger than σ_m . Second, ε is the user-specified uniform bound and generally a small constant is desired to minimize tracking error. Third, the j^{th} component of the worst case disturbance $w_M(\star)_j$ is certainly smaller than $\|w_M(\star)\|$. Therefore, ignoring the term involving ε (which is generally small), ARMOUR's robust input bound (99) is smaller than (188) by at least a factor of $\sqrt{\frac{\sigma_M}{\sigma_m}}$.

To give an idea of the magnitudes of these differences, we use the values of the parameters for the Kinova Gen3 robot as reported in Sec. X-A7. These are $\alpha_c = 1$, $\varepsilon = 0.049089$, $\sigma_M = 18.2726$, and $\sigma_m = 8.2993$. Plugging in yields

$$\frac{\alpha_c \varepsilon (\sigma_M - \sigma_m) + \|w_M(\star)\| + w_M(\star)_j}{2} \leq 0.4895 + \|w_M(\star)\|, \quad (192)$$

and

$$\|w_M(\star)\| \sqrt{\frac{\sigma_M}{\sigma_m}} = 1.48380 \|w_M(\star)\|. \quad (193)$$